HEALTH AND MEDICINE

Circulating hemopexin modulates anthracycline cardiac toxicity in patients and in mice

Jing Liu[1], Sarah Lane[1], Rahul Lall[1], Michele Russo[2], Laurie Farrell[1], Melis Debreli Coskun[3], Casie Curtin[1], Raquel Araujo-Gutierrez[4], Marielle Scherrer-Crosbie[5], Barry H. Trachtenberg[4], Jonghan Kim[3], Emanuela Tolosano[2], Alessandra Ghigo[2], Robert E. Gerszten[1], Aarti Asnani[1]*

Anthracyclines such as doxorubicin (Dox) are effective chemotherapies, but their use is limited by cardiac toxicity. We hypothesized that plasma proteomics in women with breast cancer could identify new mechanisms of anthracycline cardiac toxicity. We measured changes in 1317 proteins in anthracycline-treated patients (n = 30) and replicated key findings in a second cohort (n = 31). An increase in the heme-binding protein hemopexin (Hpx) 3 months after anthracycline initiation was associated with cardiac toxicity by echocardiography. To assess the functional role of Hpx, we administered Hpx to wild-type (WT) mice treated with Dox and observed improved cardiac function. Conversely, $Hpx^{-/-}$ mice demonstrated increased Dox cardiac toxicity compared to WT mice. Initial mechanistic studies indicate that Hpx is likely transported to the heart by circulating monocytes/macrophages and that Hpx may mitigate Dox-induced ferroptosis to confer cardioprotection. Together, these observations suggest that Hpx induction represents a compensatory response during Dox treatment.

INTRODUCTION

Anthracyclines such as doxorubicin (Dox) are highly effective antitumor chemotherapeutic agents that are commonly used for the treatment of leukemia, lymphoma, sarcoma, and some types of breast cancer (*1*). However, the use of anthracyclines is limited by dose-dependent cardiomyopathy, which occurs in about 10% of all patients and up to 20% of patients who are elderly, have preexisting cardiovascular diseases, or undergo concurrent treatment with other cardiotoxic modalities such as human epidermal growth factor receptor 2 (HER2)–targeted treatment or chest irradiation (*2*). Anthracycline-associated heart failure confers a poor prognosis (*3*), and timely diagnosis is essential to minimize adverse cardiac remodeling. However, current risk stratification and cardioprotective strategies are inadequate in patients treated with anthracyclines. Advanced imaging techniques to detect subclinical cardiac toxicity, including echocardiographic assessment of global longitudinal strain (GLS) and cardiac magnetic resonance imaging, require dedicated expertise and are unlikely to be cost-effective for screening in the growing population of patients with cancer. Conventional blood biomarkers such as cardiac troponins are often elevated after cytotoxic chemotherapy (*4*, *5*), but they are not consistently associated with the development of chronic cardiomyopathy and do not directly reflect the molecular drivers of chemotherapy-associated cardiac toxicity. Similarly, cardioprotective strategies for patients on chemotherapy rely on nonspecific neurohormonal blockade that is largely extrapolated from other types of heart failure. Given the increasing burden of both heart failure and cancer in the aging population, the development of new biomarkers and cardioprotective strategies will be essential to minimize the impact of cancer therapy–associated cardiac toxicity.

Hemopexin (Hpx) is a 57-kDa circulating glycoprotein synthesized in the liver that has a high binding affinity (K_d < 1 pmol) for the iron-containing molecule heme, which is pro-oxidant and inflammatory (*6*). Upon binding to heme, Hpx undergoes receptor-mediated endocytosis via low-density lipoprotein receptor–related protein 1 (LRP-1/CD91), which is expressed by circulating macrophages and enables heme recycling in the reticuloendothelial system in the spleen (*7*). Recent studies have highlighted the potential therapeutic role of exogenous Hpx in preventing heme-induced endothelial toxicity and cardiomyopathy in mouse models of sickle cell disease (SCD) (*8*, *9*). Although intracellular iron has been well established as a mediator of anthracycline cardiac toxicity (*10*), heme metabolism has not been previously investigated in this context. In this study, we identified induction of circulating Hpx as a cardioprotective mechanism relevant to both patients and mice treated with anthracyclines.

RESULTS

Plasma proteomics in patients identifies Hpx as a potential mediator of anthracycline cardiac toxicity

Clinical characteristics of the discovery cohort (n = 30) are summarized in Table 1. Because the left ventricular ejection fraction (LVEF) remained normal in all patients at 3 months following the initiation of anthracyclines, we instead focused on change in GLS as a marker of early cardiac toxicity. Across the cohort, GLS (absolute value) decreased by a mean of 14% at 3 months; cardiac toxicity has been defined as a relative decrease from baseline of 12% or more (*11*). Six patients developed symptoms of heart failure during the first year after anthracycline therapy, as adjudicated by a clinical cardiologist. Raw data from the proteomics study are included in Supplemental Data. After including only proteins with data to support aptamer specificity (851 of 1317) (*12*–*16*), change in GLS, as

[1]Division of Cardiovascular Medicine, Department of Medicine, Beth Israel Deaconess Medical Center, Harvard Medical School, Boston, MA, USA. [2]Department of Molecular Biotechnology and Health Sciences, Molecular Biotechnology Center, "Guido Tarone," University of Torino, Torino, Italy. [3]Department of Biomedical and Nutritional Sciences, University of Massachusetts Lowell, Lowell, MA, USA. [4]Division of Advanced Heart Failure and Transplantation, Houston Methodist Heart and Vascular Center, Houston, TX, USA. [5]Division of Cardiovascular Diseases, Department of Medicine, Hospital of the University of Pennsylvania, Philadelphia, PA, USA.
*Corresponding author. Email: aasnani@bidmc.harvard.edu

Table 1. Baseline clinical characteristics of patients treated with anthracyclines. All patients were women. GLS, absolute value of the GLS. Continuous variables are presented as means ± SD. Categorical variables are presented as number (percent). The following clinical characteristics were different between the discovery and validation cohorts when compared using the chi-square test: Dox treatment ($P = 0.04$), epirubicin treatment ($P = 0.04$), trastuzumab treatment ($P < 0.0001$), radiotherapy ($P = 0.04$), hyperlipidemia ($P = 0.002$), heart rate ($P = 0.03$), heart failure symptoms ($P = 0.04$), and baseline GLS ($P = 0.004$). LVEF, left ventricular ejection fraction. ACE, angiotensin-converting enzyme.

Clinical characteristics	Discovery cohort ($n = 30$)	Validation cohort ($n = 31$)
Age, years	50 ± 12	52 ± 14
Cancer treatments		
Doxorubicin (240 mg/m^2)	26 (87)	31 (100)
Epirubicin (300 mg/m^2)	4 (13)	0 (0)
Cyclophosphamide	30 (100)	31 (100)
Taxane	30 (100)	30 (97)
Trastuzumab	30 (100)	5 (16)
Radiotherapy	17 (57)	25 (81)
Type of cancer		
Right breast cancer	10 (33)	11 (35)
Left breast cancer	18 (60)	18 (58)
Bilateral breast cancer	2 (7)	1 (3)
Endometrial cancer	0 (0)	1 (3)
Cardiovascular risk factors		
Hypertension	12 (40)	11 (35)
Diabetes mellitus	1 (3)	5 (16)
Hyperlipidemia	8 (27)	10 (32)
Smoking	2 (7)	4 (13)
Cardiovascular treatments		
β-blocker	3 (20)	5 (16)
ACE inhibitor	5 (17)	11 (35)
Body mass index, kg/m^2	26 ± 4	29 ± 8
Systolic blood pressure, mm Hg	120 ± 18	128 ± 17*
Diastolic blood pressure, mm Hg	72 ± 10	73 ± 10*
Heart rate, beats/min	69 ± 8	73 ± 10†
Heart failure symptoms	6 (20)	1 (3)
Echocardiographic parameters		
Baseline LVEF	0.64 ± 0.05	0.63 ± 0.04
Maximum decline in LVEF	0.11 ± 0.07	0.05 ± 0.07
Time to maximum decline, months	9 ± 4	5 ± 3
Baseline GLS	21 ± 2	19 ± 3
Percent decline in GLS at 3 months	14 ± 11	0.5 ± 15

*Available in 28 patients. †Available in 26 patients.

measured by echocardiography at 3 months, was associated with relative changes in a total of 39 plasma proteins with nominal significance, as measured at either 3 or 6 months (Table 2). In this small discovery cohort, no changes were significant ($P < 0.05$) after correction for the false discovery rate. Change in GLS at 3 months was most strongly associated with the change in Hpx at 3 months ($r = -0.59$; nominal $P = 0.0005$; Table 2 and Fig. 1A), a trend that was also seen with change in Hpx at 6 months ($P = 0.086$). Of the five patients with the greatest increase in Hpx, three developed signs or symptoms of heart failure. We also observed changes in plasma proteins at nominal significance that have been previously reported in the setting of anthracycline cardiac toxicity with a similar direction of change, including neuregulin-1 (NRG1) (*17*), glutathione *S*-transferase P1 (GSTP1) (*18*), and interleukin receptor 1 antagonist (IL1RA) (*19*). As Hpx is primarily expressed in the liver, we reviewed blood metabolite profiling studies performed previously in this patient cohort (*20*). We did not observe evidence of Dox-associated hepatic injury that could explain an increase in Hpx levels in the blood or that correlated with change in GLS (see Supplemental Data).

Using a commercially available enzyme-linked immunosorbent assay (ELISA), plasma Hpx levels were then measured at baseline (before chemotherapy) and 6 weeks after the initiation of anthracyclines in the validation cohort ($n = 31$; Table 1). Hpx was similarly associated with a decline in the absolute value of GLS at 3 months, representing early cardiac toxicity ($r = -0.58$; $P = 0.0006$; Fig. 1B). Results were unchanged when only patients with breast cancer were included (see Supplemental Data). Although absolute levels of plasma Hpx were not different before and after chemotherapy in the cohort as a whole (Fig. 1C), those patients with the lowest concentrations of circulating Hpx at baseline had the biggest decline in early cardiac function following anthracyclines, as measured by change in GLS ($r = 0.63$; $P = 0.0001$; Fig. 1D).

Hpx is induced in early anthracycline cardiac toxicity in mice

Motivated by these human findings, we leveraged a mouse model that recapitulates the chronic cardiomyopathy observed in patients (Fig. 2A) (*21*). Treatment with Dox in this model resulted in a decrease in the heart weight–to–tibia length ratio (HW/TL; Fig. 2B) and a decrease in fractional shortening (FS) of 16.2% on average (50.9 ± 1.5% versus 34.7 ± 2.4%), as assessed by echocardiography 7 to 10 weeks following Dox initiation (Fig. 2, C and D). As there was no substantial difference in FS between male and female mice treated with Dox (fig. S1), male mice were used for all subsequent experiments. The heart rate was similar between control and Dox mice as measured at the time of echocardiography (mean of 797.3 beats/min versus 783.5 beats/min; $P = 0.8$). As in patients, plasma Hpx was elevated in mice within 24 hours after completion of Dox treatment (Fig. 2E) and was strongly associated with subsequent echocardiographic parameters (Fig. 2, F to H).

Because Hpx has been previously described as an acute-phase reactant induced by interleukin-6 (IL-6) (*6*, *22*), we investigated the possibility that Hpx levels increased in response to abdominal inflammation in the intraperitoneal injection model. Wild-type (WT) mice were therefore treated with Dox (5 mg/kg, intravenously) or saline once weekly for 4 weeks via tail vein, a regimen that has previously been shown to cause chronic cardiomyopathy (*23*). Plasma Hpx levels in mice treated with Dox increased with serial

Table 2. Associations between changes in proteins at 3 or 6 months after anthracyclines and change in GLS at 3 months in the breast cancer discovery cohort. FAP, fibroblast activation protein; BDNF/INT-3, brain-derived neurotrophic factor/neurotrophin-3; EGF, epidermal growth factor.

Protein	Pearson's *R* 3 months (*n* = 30)	Nominal *P* value	Pearson's *R* 6 months (*n* = 12)	Nominal *P* value	Data supporting aptamer specificity
Hemopexin	−0.59	5.0×10^{-4}	−0.52	8.6×10^{-2}	†
E-selectin	0.53	2.5×10^{-3}	−0.18	0.6	*, †, ‖
Interleukin-17D	0.52	3.1×10^{-3}	0.00	1.0	*
Contactin-1	0.50	5.1×10^{-3}	0.27	0.4	*, †, ‖
Interleukin-17 receptor A	−0.49	6.4×10^{-3}	−0.24	0.5	*, †, ‡, §, ‖
Serum amyloid P-component	−0.47	9.3×10^{-3}	0.34	0.3	*, †, ‡, §
Creatine kinase B-type	0.47	9.4×10^{-3}	0.40	0.2	*, †
CD209 antigen	0.46	1.0×10^{-2}	0.13	0.7	*, †, ‡, §
Ribonuclease H1	0.45	1.3×10^{-2}	0.13	0.7	*
Neurogenic locus notch homolog protein 3	0.45	1.3×10^{-2}	0.02	1.0	*, †, ‖
Netrin-4	0.44	1.4×10^{-2}	−0.01	1.0	*, †, §
Galactoside 3(4)-L-fucosyltransferase	−0.44	1.4×10^{-2}	0.15	0.6	*, †, ‡, §
Neuregulin-1	0.44	1.4×10^{-2}	−0.24	0.5	*
Plexin-C1	0.44	1.6×10^{-2}	0.24	0.5	*, †, ‡, §
Casein kinase II 2-α:2-β heterotetramer	−0.44	1.6×10^{-2}	0.15	0.6	*
Leptin	0.43	1.7×10^{-2}	0.23	0.5	†, ‖
Prolyl endopeptidase FAP	0.43	1.8×10^{-2}	−0.05	0.9	*
Dynein light chain roadblock-type 1	−0.43	1.8×10^{-2}	0.24	0.5	†
Glutathione *S*-transferase P1	−0.42	1.9×10^{-2}	−0.11	0.7	*, †, §
Leukocyte immunoglobulin-like receptor subfamily B member 1	0.42	2.2×10^{-2}	−0.20	0.5	*, †, ‡, §
Mannose-binding protein C	−0.41	2.4×10^{-2}	−0.54	7.1×10^{-2}	*, †, ‡, §, ‖
C-type lectin domain family 4 member K	−0.40	2.7×10^{-2}	−0.16	0.6	*, †, §
Platelet glycoprotein Ib α chain	−0.40	2.8×10^{-2}	−0.19	0.5	*, †, §
BDNF/NT-3 growth factors receptor	0.40	2.9×10^{-2}	0.13	0.7	*
Contactin-2	0.40	2.9×10^{-2}	0.13	0.7	*, †, ‡, §
Prolactin	0.40	3.0×10^{-2}	−0.51	9.0×10^{-2}	*
C-C motif chemokine 16	−0.40	3.1×10^{-2}	−0.01	1.0	*, †, ‡, §, ‖
Junctional adhesion molecule-like	0.40	3.1×10^{-2}	−0.13	0.7	†, §
C-C motif chemokine 27	−0.39	3.5×10^{-2}	−0.26	0.4	*, †
Somatotropin	0.38	3.7×10^{-2}	0.09	0.8	*, †
Follistatin-related protein 1	0.37	4.3×10^{-2}	−0.25	0.4	*, †, §
Teratocarcinoma-derived growth factor 1	0.37	4.4×10^{-2}	−0.21	0.5	*, †, ‡, §
L-Selectin	0.37	4.5×10^{-2}	−0.31	0.3	*, †, ‡, §, ‖
Interleukin-6 receptor subunit α	0.37	4.7×10^{-2}	−0.36	0.3	*, †, ‡, §, ‖
EGF-containing fibulin-like extracellular matrix protein 1	0.36	4.8×10^{-2}	−0.12	0.7	*, †, §
Interleukin-1 receptor antagonist protein	−0.03	0.9	−0.72	8.6×10^{-3}	*, †, §, ‖
Tumor necrosis factor receptor superfamily member 10A	0.01	1.0	0.67	1.8×10^{-2}	*
Angiogenin	−0.32	8.2×10^{-2}	−0.63	3.0×10^{-2}	*, †, ‡, ‖
Apolipoprotein B	−0.32	8.6×10^{-2}	−0.59	4.2×10^{-2}	*, †, ‡

*Benson *et al*. (*16*); meta-analysis $P < 1.0 \times 10^{-6}$. †Emilsson *et al*. (*13*); $P < 5.0 \times 10^{-8}$. ‡Suhre *et al*. (*14*). §Sun *et al*. (*15*). ‖Olink platform; Pearson correlation > 0.6.

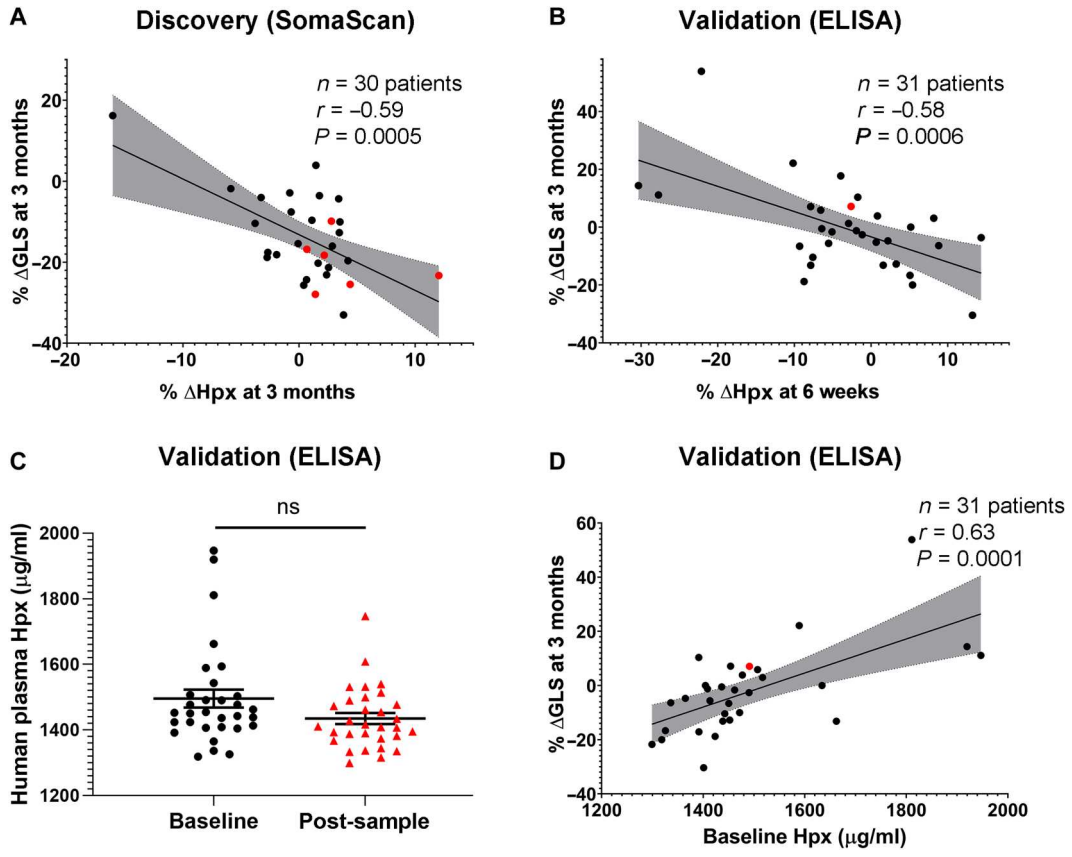

Fig. 1. Circulating Hpx levels in two patient cohorts. (**A** and **B**) Change in plasma Hpx as measured between 6 weeks and 3 months following initiation of anthracyclines was associated with change in GLS (absolute value) at 3 months in patients with breast cancer enrolled in the discovery and validation cohorts, respectively. (**C**) Absolute value of plasma Hpx at baseline (before anthracyclines) and at 6 weeks following the initiation of anthracyclines in the validation cohort, as measured by ELISA. (**D**) Baseline plasma Hpx concentration was associated with change in GLS at 3 months. All patients were treated with dose-dense doxorubicin and cyclophosphamide (ddAC). Patients denoted in red developed symptoms of heart failure. Pearson's correlation coefficient was used to compare percent change in ΔHpx or baseline Hpx to percent change in ΔGLS. ns indicates that there was no significant difference between the groups.

injections in both intraperitoneal and intravenous models, peaking at day 7 and week 4, respectively (fig. S2, A and B). Similarly, although plasma IL-6 increased in response to Dox treatment in the intraperitoneal model (fig. S2C), IL-6 levels did not correlate with cardiac function on subsequent echocardiography (fig. S2D). In patients enrolled in the discovery cohort, changes in other acute-phase reactants (C-reactive protein, serum amyloid A, alpha1-antitrypsin, and haptoglobin) did not correlate with change in GLS (fig. S2E). Therefore, although Hpx has been reported as an acute-phase reactant, our human and mouse findings did not support the notion that Hpx is simply a nonspecific marker of inflammation in the context of anthracycline treatment.

Hpx protects against anthracycline cardiac toxicity

Because Hpx is cardioprotective in mouse models of heme overload (*8*, *9*), we treated WT mice that received Dox or saline with purified human Hpx protein or corresponding vehicle (saline; Fig. 3A). Human Hpx protein has been previously shown to decrease heme loading in mouse models of SCD and β-thalassemia at the selected dose (700 μg in 1.2- to 2.0-ml plasma volume per mouse) (*8*), which approximates physiologic concentrations of circulating Hpx (1 to 2 mg/ml; Fig. 2E). Western blotting using an antibody to human Hpx demonstrated an increase in Hpx protein in the heart, as shown in fig. S3. Administration of Hpx prevented the development of Dox-induced cardiac dysfunction as assessed by echocardiography 7 weeks after Dox initiation (Fig. 3, B and C). Wheat germ agglutinin (WGA) staining of heart sections showed that Dox decreased cardiomyocyte size, an effect that was mitigated by Hpx treatment (Fig. 3, D and E). In addition, Dox induced the expression of brain-type natriuretic peptide (*Nppb*) and the *Bax/Bcl2* ratio, markers of cardiac stress and apoptosis, respectively. Hpx treatment abrogated Dox-induced expression of *Nppb* ($P = 0.001$) with a similar trend observed for *Bax/Bcl2* (Fig. 3, F and G).

We then administered Dox to Hpx-deficient ($Hpx^{-/-}$) mice using the treatment strategy illustrated in Fig. 2A. Male $Hpx^{-/-}$ mice treated with Dox developed severe systemic illness requiring early euthanasia (Fig. 4A). Therefore, the chronic cardiomyopathy phenotype could not be evaluated in this model. However, in mice euthanized within 24 hours after completion of the 2-week Dox regimen, we observed smaller cardiomyocyte size and increased brain type natriuretic peptide (*Nppb*) and apoptotic factors (*Bax/Bcl2* ratio and cleaved caspase-3) in the hearts of $Hpx^{-/-}$ mice compared to WT mice, suggesting increased cardiac stress and apoptosis in mice lacking Hpx (Fig. 4, B to E, and fig. S4). Some of these

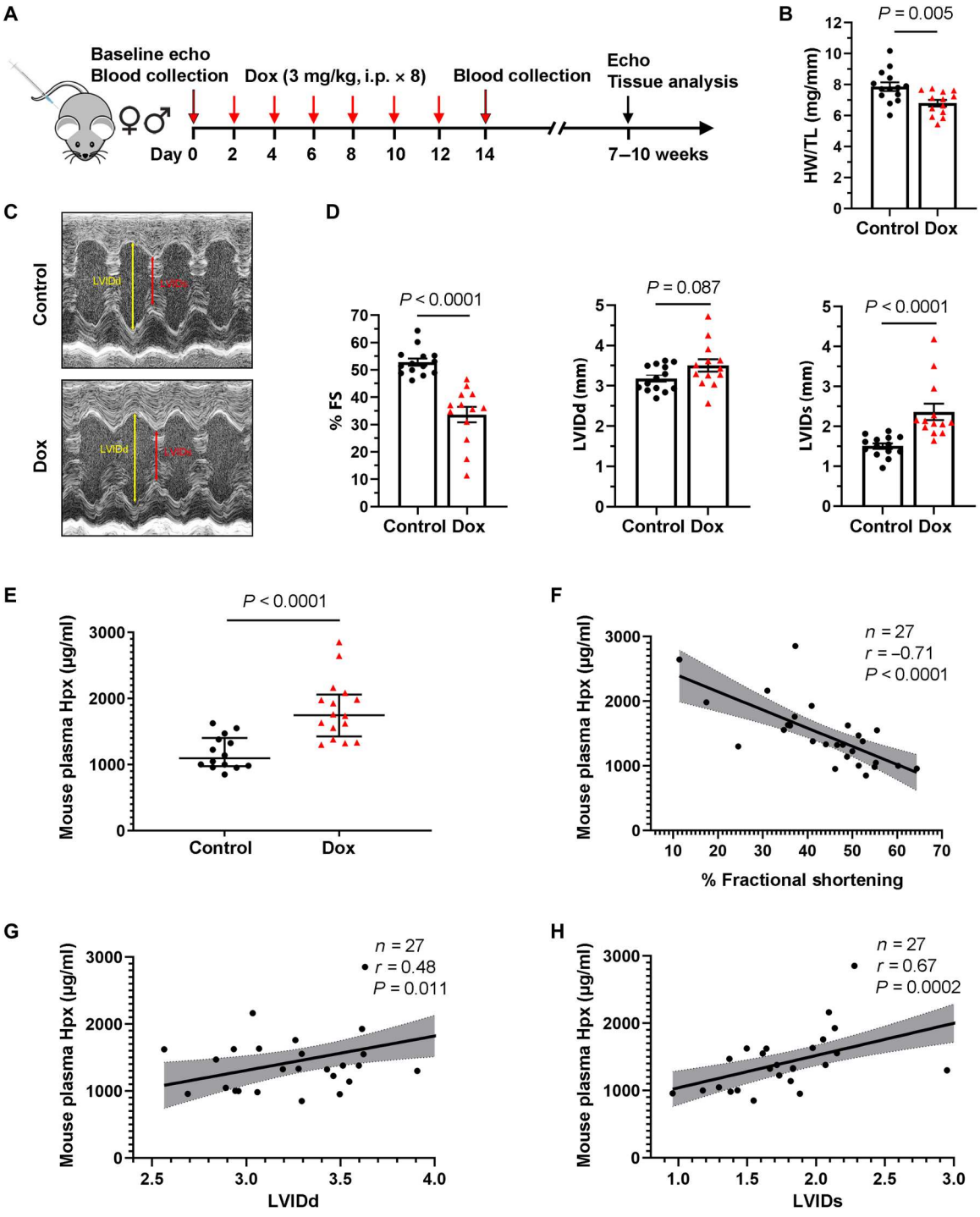

Fig. 2. Circulating Hpx is elevated in mice treated with Dox. (**A**) Dox-induced chronic cardiomyopathy model in mice. i.p., intraperitoneally. (**B**) Heart weight (HW)/tibia length (TL) ratio in saline-treated (control) and Dox-treated (Dox) groups. (**C**) Representative images of control and Dox mice obtained during conscious echocardiography. (**D**) Cardiac function at 5 to 8 weeks after Dox treatment: FS, LVIDd, and LVIDs in control and Dox groups. FS, fractional shortening. (**E**) Absolute levels of mouse plasma Hpx following treatment in control and Dox groups. (**F** to **H**) Absolute levels of mouse plasma Hpx after treatment were associated with change in % FS, LVIDd, and LVIDs. Data were expressed as means ± SEM. Welch's *t* test was used to compare the difference between control (n = 14) and Dox-treated (n = 13) groups. Pearson's correlation coefficient was used in (F) to (H).

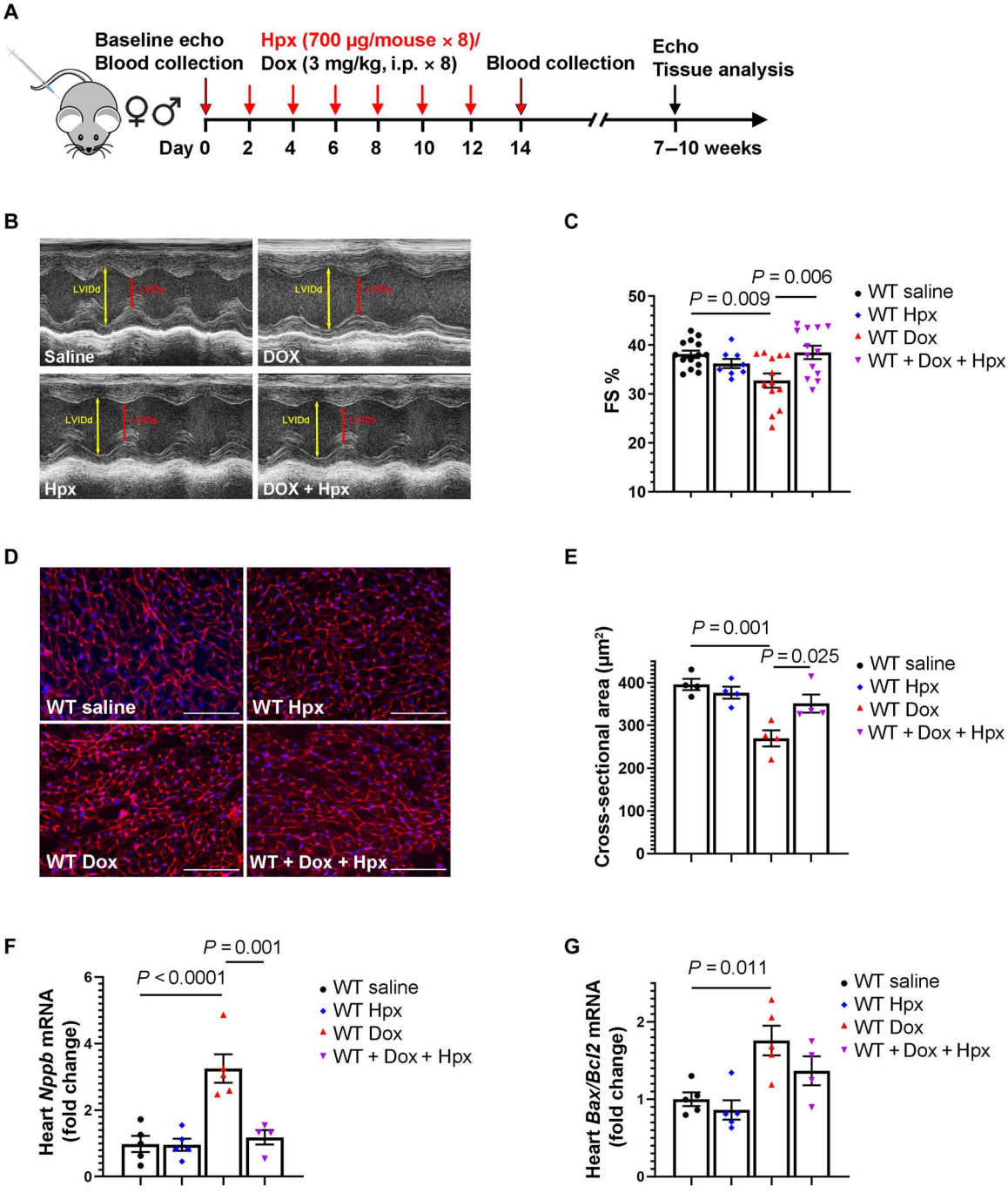

Fig. 3. Treatment with exogenous Hpx protects against anthracycline cardiac toxicity. (**A**) Mouse treatment protocol. (**B**) Representative images obtained during sedated echocardiography. (**C**) FS % at 5 weeks after Dox or Hpx treatment. $n = 15$ for WT saline group, $n = 9$ for WT/Hpx group, $n = 13$ for WT/Dox group, and $n = 13$ for WT/Dox + Hpx group. (**D**) Representative images of WGA staining in the heart. Scale bars, 100 μm. (**E**) Cardiomyocyte cross-sectional area in WT mice treated with saline, Hpx, Dox, or Dox + Hpx. $n = 4$ per group. (**F** and **G**) Cardiac *Nppb* ($n = 5, 5, 5$, and 4, respectively) and *Bax*/*Bcl2* ratio ($n = 5, 5, 5$, and 4, respectively) measured by reverse transcription quantitative polymerase chain reaction (RT-qPCR) within 24 hours after completion of the 2-week Dox regimen. Data were expressed as means ± SEM. Ordinary one-way analysis of variance (ANOVA) followed by the Tukey-Kramer test was used to compare the means of experimental groups.

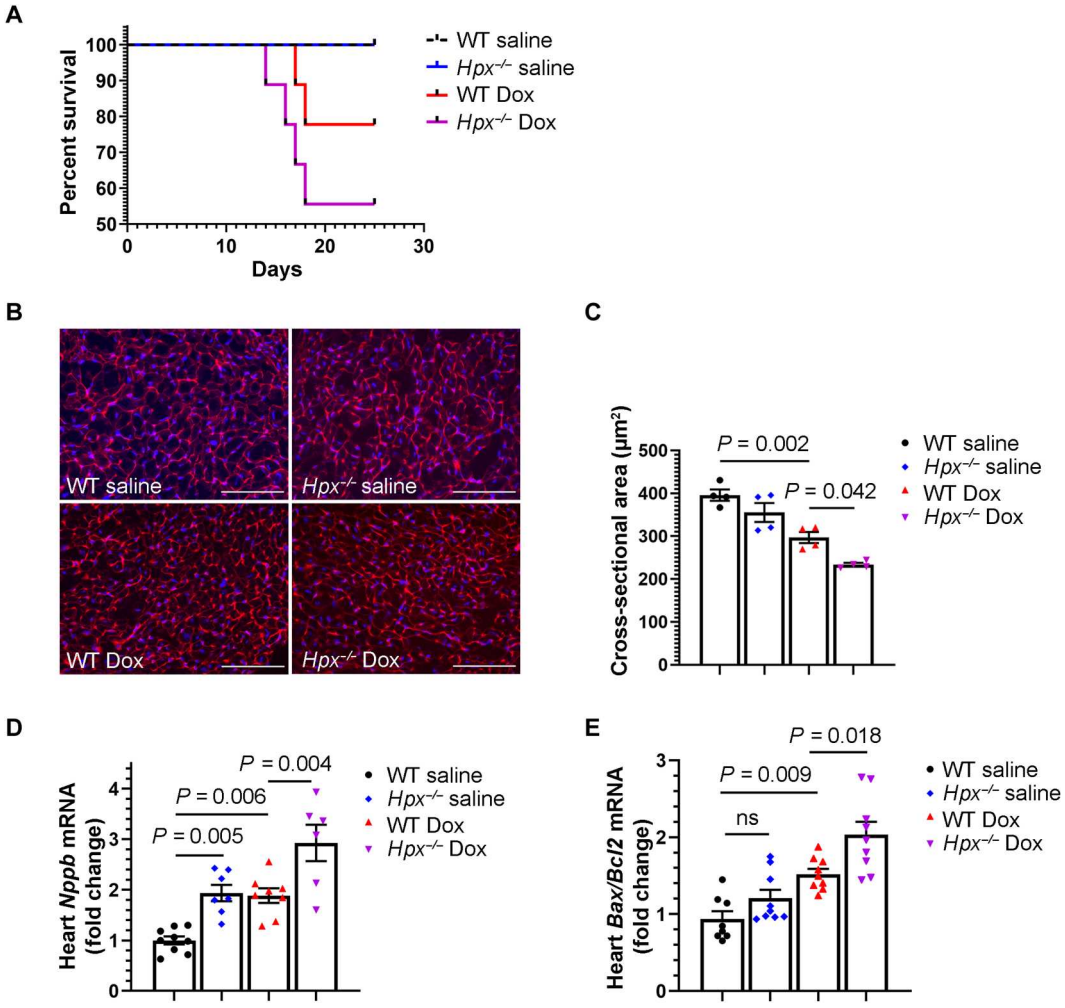

Fig. 4. Hpx deficiency exacerbates anthracycline cardiac toxicity. (**A**) Survival curves of WT and $Hpx^{-/-}$ mice treated with saline or Dox. (**B**) Representative images of WGA staining in the heart. Scale bars, 100 μm. (**C**) Cardiomyocyte cross-sectional area in WT mice or $Hpx^{-/-}$ mice treated with saline or Dox, respectively. $n = 4$ per group. (**D** and **E**) Cardiac *Nppb* ($n = 9$, 7, 8, and 6, respectively) and *Bax*/*Bcl2* ratio ($n = 8$, 9, 9, and 9, respectively) measured by RT-qPCR within 24 hours after completion of the 2-week Dox regimen. Data were expressed as means ± SEM. Ordinary one-way ANOVA followed by the Tukey-Kramer test was used to compare the means of experimental groups.

pathways also appeared to be dysregulated in $Hpx^{-/-}$ mice treated with saline, although baseline cardiac function (pre-Dox) was normal in $Hpx^{-/-}$ mice (fig. S5). Together, these data support Hpx induction as a cardioprotective and potentially compensatory response to Dox cardiac toxicity.

Hpx-mediated cardioprotection is not primarily regulated by heme or nonheme iron

We next hypothesized that Hpx induction may occur in response to increased circulating heme levels. However, whole blood and plasma heme levels were decreased in Dox mice relative to control mice after 2 weeks of treatment, an effect that was independent of the presence or absence of Hpx (Fig. 5, A and B). A similar decrease in heme levels was observed in the livers and in hearts of mice treated with Dox (Fig. 5, C and D). Hpx deletion mitigated this effect in the heart, suggesting that Hpx is important in cardiac heme recycling in the context of Dox treatment. Dox treatment was also associated with an increase in nonheme iron (NHI) in the liver but not in the heart (Fig. 5, E and F), an effect that was independent of Hpx.

Hpx's role in the heart may be mediated by circulating leukocytes

To study the biology of Hpx-associated cardioprotection, we first assessed *Hpx* in the heart and in the liver, which is the primary site of Hpx expression (*7*). Dox-mediated induction of *Hpx* at 2 weeks, as measured by reverse transcription quantitative polymerase chain reaction (RT-qPCR), was pronounced in the liver but not in the heart (Fig. 6A). However, we were interested to find that Hpx protein level was markedly increased in the hearts of mice treated with Dox compared to saline controls, as assessed by Western blot (Fig. 6B). These findings suggest that Hpx may be transported to the heart from the circulation. Consistent with these observations, we noted that the Hpx receptor, LRP-1, did not colocalize with cardiac endothelial cells or cardiomyocytes when assessed by immunofluorescence staining (fig. S6). As LRP-1 has been reported

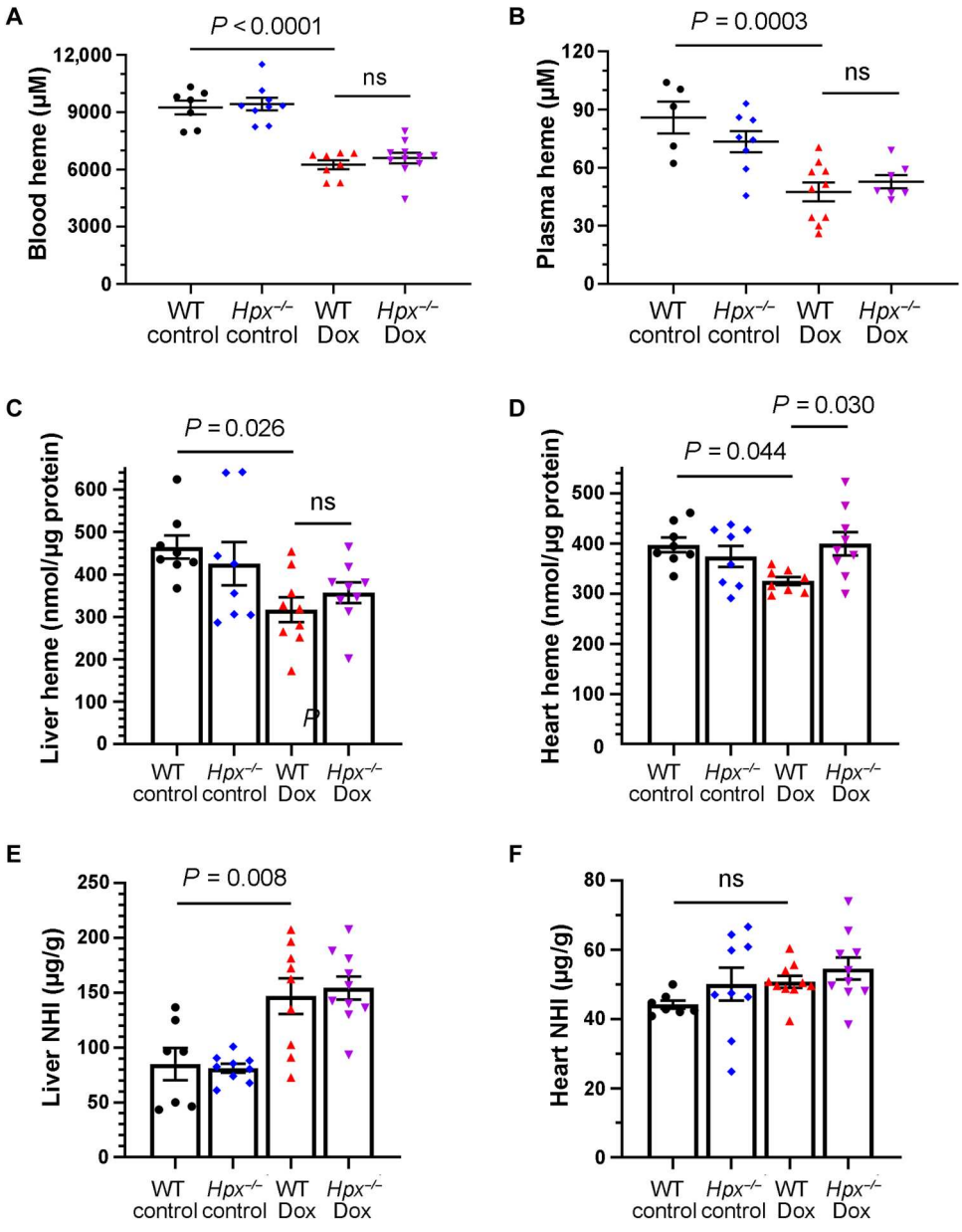

Fig. 5. Regulation of heme and NHI in Dox cardiac toxicity. (**A** to **D**) Heme levels in whole blood ($n = 7$ to 11 per group) (A), plasma ($n = 5$ to 10 per group) (B), liver ($n = 7$ to 10 per group) (C), and heart ($n = 8$ to 9 per group) (D) as measured within 24 hours after completion of the 2-week Dox regimen in mice. (**E** and **F**) NHI in the liver ($n = 7$ to 10 per group) (E) and heart ($n = 7$ to 10 per group) (F) within 24 hours after completion of the 2-week Dox regimen in mice. Data were expressed as means ± SEM. Ordinary one-way ANOVA followed by the Tukey-Kramer test was used to compare the means of experimental groups.

to be expressed by endothelial cells in other tissues (*24*), we assessed Hpx and LRP-1 expression in adult mouse heart endothelial cells (MHECs) treated with Dox (200 to 800 ng/ml) for 48 hours and could not detect these proteins by Western blot (Fig. 6C). Using flow cytometry to assess heart and blood leukocytes from mice treated with the chronic Dox regimen, we found that Hpx colocalized with $CD45^+$ immune cells (Fig. 6D), specifically $CD11b^+$ $CD64^+$ macrophages/monocytes in the heart and in the circulation (Fig. 6E). Immunofluorescence staining confirmed that LRP-1 colocalized with $CD64^+$ immune cells (fig. S7).

Hpx modulates cardiac inflammation in mice treated with Dox

To study the biology of macrophages in Hpx-associated cardioprotection, we first assessed whether macrophages produce Hpx. We isolated macrophages/monocytes from the circulation and from the heart in mice with and without Dox treatment. We did not observe *Hpx* mRNA expression in isolated macrophages, consistent with prior observations that the macrophage serves as a carrier of Hpx through LRP-1–mediated endocytosis rather than a primary source of Hpx expression. The macrophage sorting strategy is presented in fig. S8. We next studied macrophage phenotypes in the

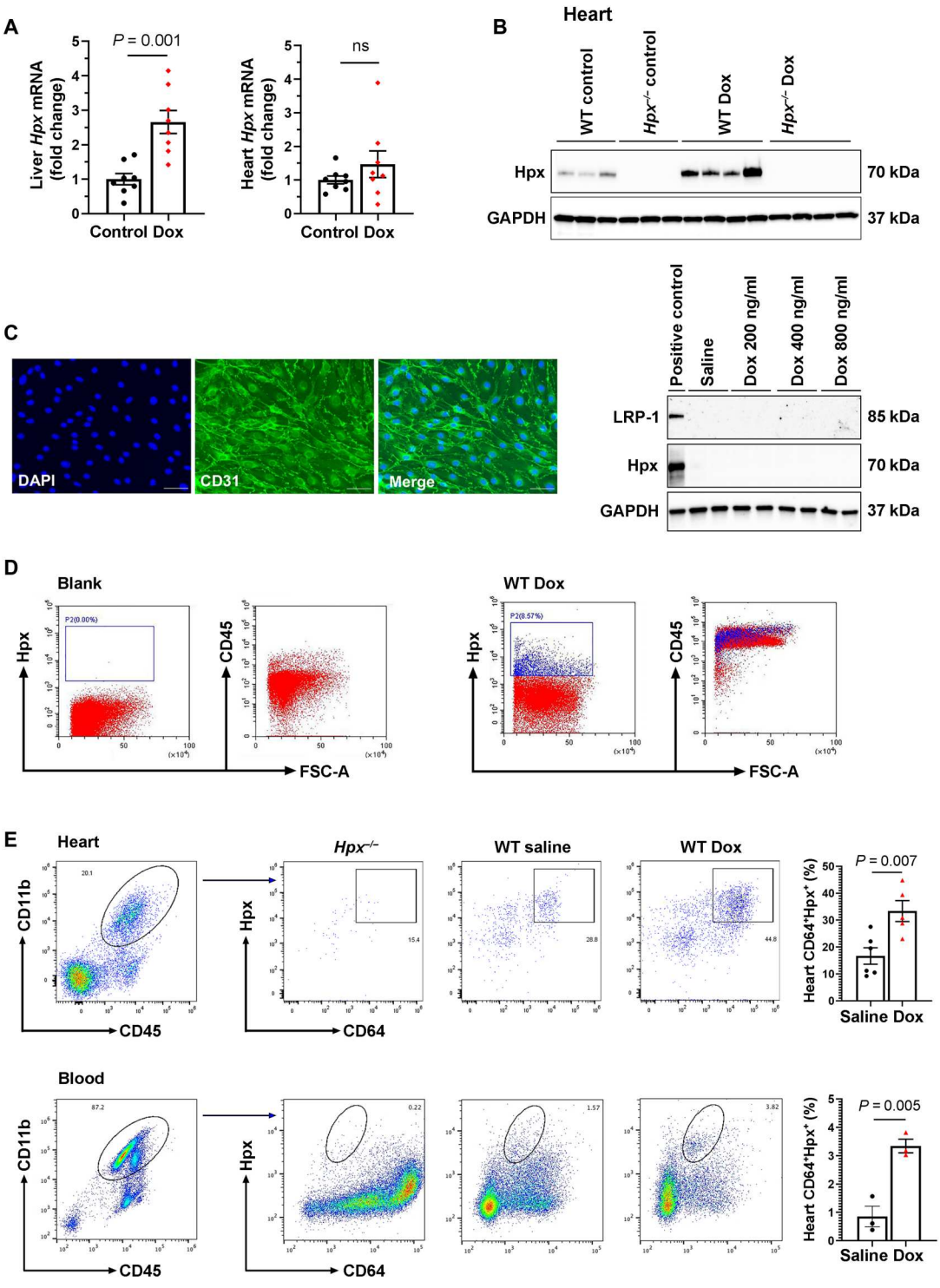

Fig. 6. Hpx may be transported to the heart by circulating macrophages. (**A**) *Hpx* mRNA levels in the liver and heart in mice treated with saline (control; $n = 8$) and Dox ($n = 8$) mice within 24 hours after completion of the 2-week regimen. (**B**) Cardiac Hpx protein level within 24 hours after completion of the 2-week regimen ($n = 8$). (**C**) Glyceraldehyde-3-phosphate dehydrogenase (GAPDH), Hpx, and LRP-1 detected by Western blot in adult MHECs treated with saline (control) or Dox at a concentration of 200, 400, and 800 ng/ml for 48 hours. The left-most lane is a liver sample that was used as a positive control. DAPI, 4′,6-diamidino-2-phenylindole. (**D**) Circulating Hpx-expressing cells were $CD45^+$ immune cells, as determined by fluorescence-activated cell sorting (FACS). FSC-A, forward scatter area. (**E**) Hpx-expressing cells were $CD11b^+$ $CD64^+$ macrophages in the heart and circulation as determined by FACS. Data were expressed as means ± SEM. Welch's *t* test was used to compare the difference between control and Dox-treated groups.

setting of Dox treatment by performing RT-qPCR to detect representative gene expression of inflammatory macrophages (*Irf5*, *CXCR2*, *Nr4a1*, and *CCL12*) versus reparative macrophages (*Emr1*, *Pdgfc*, and *Hbegf*) in heart tissue (*25*). Expression of *Irf5*, *Nr4a1*, *Emr1*, *Pdgfc*, and *Hbegf* was not different between groups, as indicated in fig. S9. However, we found that Dox induced expression of *CXCR2* and *CCL12* and that Hpx cotreatment abrogated this effect. Furthermore, Hpx-deficient mice treated with Dox demonstrated the most prominent expression of *CXCR2* and *CCL12* (Fig. 7, A to D). Together, these initial results suggest that Hpx may down-regulate Dox-induced inflammatory macrophages in the heart.

Hpx mitigates Dox-induced ferroptosis in the heart

Ferroptosis, a novel form of regulated cell death, has been previously implicated in the pathobiology of anthracycline-induced cardiomyopathy (*26*). To investigate the role of Hpx in Dox-induced ferroptosis, we first assessed malondialdehyde (MDA), a marker of lipid peroxidation, and 2′,7′-dichlorofluorescein (DCF), a marker of oxidative stress, in heart tissue. We found that Dox treatment resulted in increased lipid peroxidation and DCF in the heart, as previously described, and that Hpx deficiency exacerbated this effect with or without Dox treatment (Fig. 7, E and F). We next detected the expression of heme oxygenase–1 (HO-1) and nuclear factor erythroid 2–related factor (Nrf2), a transcription factor that regulates HO-1

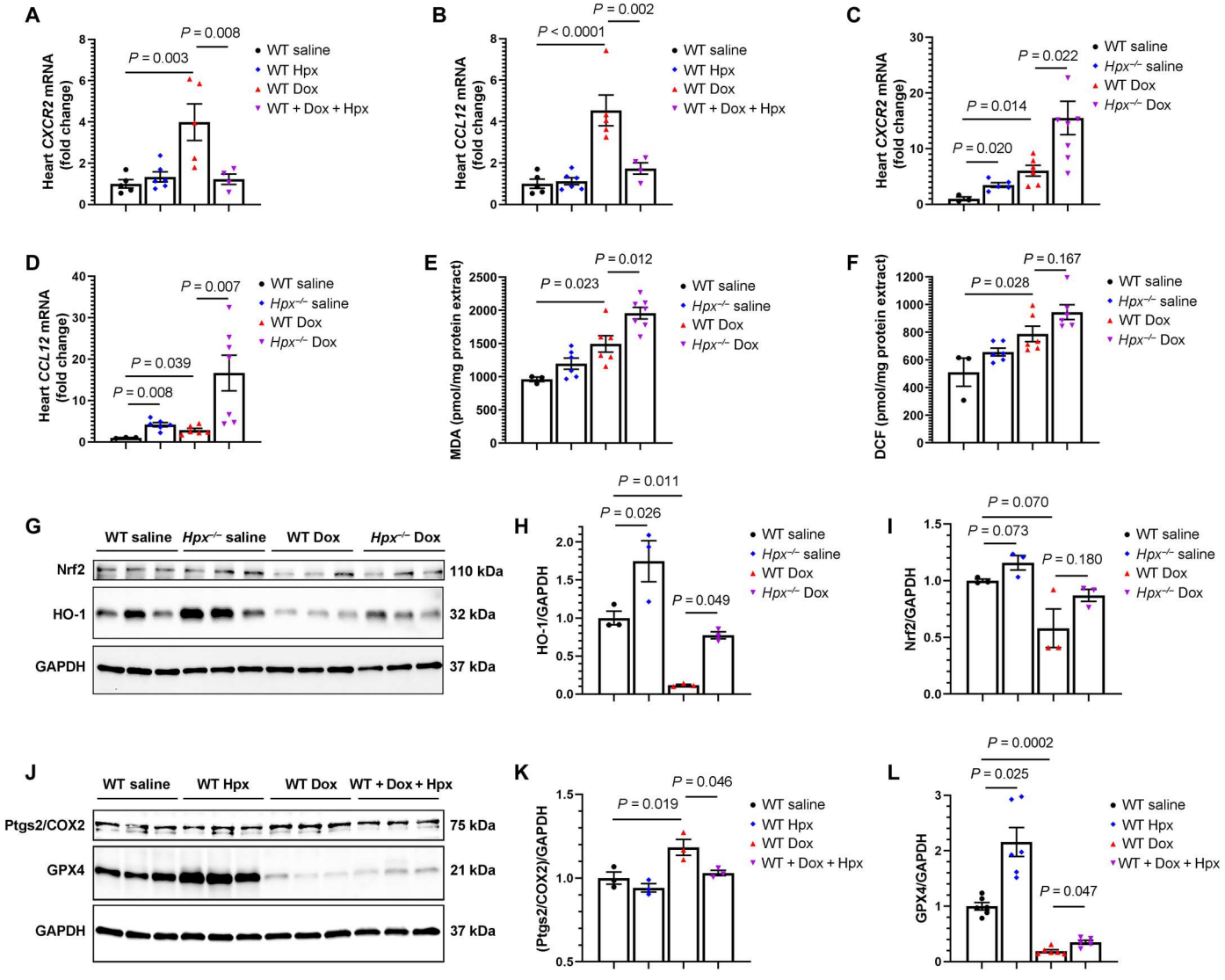

Fig. 7. Hpx modulates Dox cardiac toxicity via suppression of the inflammatory macrophage phenotype and ferroptosis. (**A** and **B**) Cardiac *CXCR2* and *CCL12* mRNA levels in the heart in WT mice treated with saline ($n = 5$), Hpx ($n = 6$), Dox ($n = 5$), and cotreatment of Dox and Hpx ($n = 4$). (**C** and **D**) *CXCR2* and *CCL12* mRNA levels in the heart in WT or *Hpx*$^{-/-}$ mice treated with saline ($n = 3$ and 6) or Dox ($n = 6$ and 7). (**E** and **F**) Malondialdehyde (MDA) levels and DCF fluorescence in the heart in WT or *Hpx*$^{-/-}$ mice treated with saline ($n = 3$ and 6) or Dox ($n = 6$ and 7). (**G**) Cardiac HO-1 and Nrf2 detected by Western blot in WT or *Hpx*$^{-/-}$ mice treated with saline or Dox ($n = 3$ per group). (**H** and **I**) Quantification of HO-1 and Nrf2. (**J**) Cardiac Ptgs2/COX2 and GPX4 detected by Western blot in WT mice treated with saline, Hpx, Dox, and cotreatment of Dox and Hpx ($n = 3$ per group). (**K** and **L**) Quantification of Ptgs2/COX2 and GPX4. GAPDH was used as loading control. All samples were harvested within 24 hours after completion of the 2-week Dox regimen. Data were expressed as means ± SEM. Ordinary one-way ANOVA followed by the Tukey-Kramer test was used to compare the means of experimental groups.

expression, by Western blot. We found that Dox reduced the expression of HO-1, whereas Hpx deficiency resulted in increased expression of HO-1 both with and without Dox treatment (Fig. 7, G and H), consistent with prior observations (*27*). A similar trend was observed with Nrf2 (Fig. 7, G and I). We further analyzed expression of prostaglandin-endoperoxide synthase 2 (Ptgs2/COX2), a biomarker of ferroptosis (*28*), and glutathione peroxidase 4 (GPX4), an antioxidative enzyme and key regulator of ferroptosis (*29*), by Western blot and RT-qPCR. We found that Dox induced the expression of Ptgs2/COX2 at both the mRNA and protein level. Hpx treatment abrogated the Dox-induced increase of Ptgs2/COX2 (Fig. 7, J and K, and fig. S10). In addition, Dox decreased the expression of GPX4 at the protein level ($P = 0.001$). Hpx treatment increased the expression of GPX4 in saline-treated mice, and a similar trend was observed with Dox treatment (Fig. 7, J and L). Together, these results suggest that Hpx protects against Dox-induced ferroptosis.

DISCUSSION

This study supports a role for Hpx induction as a cardioprotective mechanism that is activated in the setting of Dox-induced chronic cardiomyopathy. Although plasma Hpx levels in patients were associated with increased cardiac toxicity, our preclinical data suggest that higher levels of Hpx in patients treated with anthracyclines should be physiologically beneficial and cardioprotective. It is possible that circulating Hpx could serve as a diagnostic and prognostic circulating blood marker, similar to brain natriuretic peptide (BNP) in other types of heart failure. BNP is secreted in the bloodstream in response to cardiac overload, leading to natriuresis and vasodilation that, in turn, protect against the congestion that occurs in heart failure. Similarly, we postulate that circulating Hpx increased in both patients and mice in response to anthracycline-induced cardiac dysfunction. In the current work, we did not observe an increase in blood heme levels or an association between Hpx and the inflammatory acute-phase response. Future studies will focus on the factors leading to Hpx induction in patients with anthracycline-associated cardiac toxicity.

Prior work in heme-overload hemolytic diseases, such as SCD and β-thalassemia, has demonstrated that the protective effects of Hpx are mediated by heme scavenging (*8*, *9*, *30*, *31*) in the context of microvascular stasis (*32*), vaso-occlusion (*33*), and lipid oxidation (*34*). In contrast to hemolytic disorders, we observed decreased levels of circulating heme in mice at the completion of the 2-week Dox regimen, independent of the presence or absence of Hpx. One possibility is that the turnover kinetics of Hpx differs from those of circulating heme, particularly during Dox treatment. For instance, Hpx may have a longer half-life in the blood (and therefore be measured at higher levels) secondary to decreased heme (*35*). Notably, we did not observe evidence of iron deficiency based on tissue measurements of NHI in mice treated with Dox.

Our initial experiments suggest that Hpx′s effects on the heart are mediated by circulating macrophages in mice treated with Dox. This is consistent with prior reports that bone marrow–derived macrophages participate in the early phases of Dox-induced cardiac inflammation (*36*), and macrophages have been previously described to express the Hpx receptor LRP-1 (*37*, *38*). Further investigation will be necessary to elucidate the cell type and tissue specificity of Dox-mediated Hpx induction, as well as the pharmacokinetics of Hpx and heme transport in this setting. The downstream mechanisms underlying cardioprotection by Hpx-carrying macrophages and the potential for cross-talk with cardiomyocytes remain to be determined. Future experiments will aim to define mechanisms leading to cross-talk between the immune system and the myocardium in the setting of Dox treatment, including the potential role of mitochondrial transfer, which has not been well characterized in this context. Hpx-deficient mice treated with saline had increased cardiac expression of *Nppb* and HO-1, indicating that Hpx may play a role in maintaining normal cardiac homeostasis. Hence, efforts to define the role of Hpx signaling in Dox cardiac toxicity may also provide insight into the molecular pathways contributing to cardiac dysfunction in general, outside the context of anthracycline treatment.

Intracellular iron overload has been consistently reported as a mechanism of Dox cardiac toxicity in patients (*39*) and animal models (*10*, *40*) and can lead to ferroptosis, a regulated form of cell death mediated by iron-dependent lipid peroxidation and oxidative stress (*26*). HO-1 is known to catalyze heme degradation into biliverdin/bilirubin, carbon monoxide, and ferrous iron, leading to ferroptosis. The induction of HO-1 has been suggested to contribute to Dox-induced cardiac toxicity by causing heme degradation in the heart and the release of free iron, which then leads to lipid peroxidation. In this study, we found that HO-1 expression was down-regulated by Dox, rather than induced by Dox as has been previously reported (*26*). Notably, up-regulation of HO-1 was reported with the use of an acute, high-dose Dox administration protocol (single injection of 20 mg/kg, intraperitoneally), as opposed to the chronic, low-dose Dox protocol used in the current study that recapitulates treatment regimens received by patients. We hypothesize that a single high dose of Dox causes severe cellular damage, leading to brisk activation of HO-1, reactive oxygen species overload, and excessive free iron release that may not be seen with chronic, low-dose administration of Dox. Notably, HO-1 was up-regulated in Hpx-deficient mice (versus WT mice) treated with Dox, suggesting that Hpx may be important in mitigating ferroptosis in the setting of Dox.

Ferroptosis is characterized by excessive accumulation of free cellular iron, leading to lipid peroxidation and oxidative stress. Inactivation of GPX4, an antioxidant enzyme that neutralizes lipid peroxides, has been shown to promote ferroptosis (*41*, *42*). In line with this concept, induction or overexpression of GPX4 has been demonstrated to protect against oxidative damage, which, in turn, inhibits ferroptosis (*43*). PTGS2, also known as COX2, metabolizes arachidonic acid into prostaglandins and is considered to be a downstream marker of ferroptosis (*43*). Although a causative role for PTGS2 in ferroptosis has not been clearly established, down-regulation of PTGS2 mRNA in a traumatic brain injury mouse model prevented ferroptotic neuronal death (*44*). In our study, Hpx treatment was associated with increased GPX4 and decreased PTGS2 in mouse cardiac tissue, both with and without Dox treatment. These observations are consistent with prior data from our group showing that Hpx mitigates ferroptosis in the setting of heme overload (*9*).

Our group and others have implicated several additional molecular pathways based on preclinical models of anthracycline cardiac toxicity, including autophagy and mitophagy (*21*, *45*), activation of the aryl hydrocarbon receptor and cytochrome P450 enzymes (*18*, *46*), Dox′s interaction with the β isoform of topoisomerase II (Top2β) (*47*), and tissue-specific modulation of apoptotic factors (*21*). As multiple mechanisms likely contribute to Dox cardiac

toxicity, additional experiments will be necessary to assess the ways in which Hpx signaling may interact with previously described molecular pathways.

It is imperative that novel strategies to protect the heart during cancer therapy maintain a neutral effect or ideally potentiate the antitumor activity of cancer therapy. An inverse relationship between plasma heme and Hpx levels was recently reported in patients with prostate cancer (*48*). Heme promoted tumor growth and metastasis in mouse models, an effect that was attributed to heme's role in regulating the oncogene *c-MYC*. *Hpx*$^{-/-}$ mice demonstrated the most aggressive tumor phenotypes, suggesting that augmentation of Hpx could simultaneously protect the heart and limit tumor growth. Hpx treatment has not yet been evaluated as an antitumor strategy in malignancies that are typically treated with anthracyclines. Future studies will be necessary to define the effects of modulating Hpx on cancer outcomes, both in tumor xenograft mouse models and in patients receiving anthracycline therapy.

In this study, the initial discovery cohort used for proteomics was enriched for patients who demonstrated overt cardiac toxicity, with 6 of 30 patients (20%) showing signs or symptoms of heart failure. According to prior data, approximately 4% of patients treated with modern-day anthracycline dosing go on to develop symptomatic heart failure (*49*). Consistent with published observations, only 1 of 31 patients (3%) developed symptomatic heart failure in the real-world validation cohort. Additional studies will be necessary to assess the sensitivity and specificity of Hpx as a cardiac toxicity biomarker in patients, as well as the optimal patient population and timing of blood sample collection relative to anthracycline treatment. Notably, we found that both baseline levels of Hpx and changes in Hpx over time were associated with early cardiac toxicity, suggesting that interindividual differences in Hpx biology could potentially be leveraged for improved cardiac risk stratification in patients planned for anthracycline treatment.

In the discovery cohort, we also observed changes in other plasma proteins associated with the development of anthracycline cardiac toxicity, including NRG1, GSTP1, and IL1RA. NRG1 represents the neuregulin/ErbB pathway that is activated in response to cardiac stress, including during anthracycline treatment (*17*). Circulating NRG has been previously reported to decrease following anthracycline treatment, as seen in our cohort. GSTP1 represents an essential antioxidant pathway. We previously found that GSTP2, a homologous protein in zebrafish, increased in response to anthracyclines (*18*). Last, IL1RA, representing activation of IL-1, was previously found to be increased in mice with Dox cardiac toxicity (*19*). It remains unclear whether changes in Hpx and other circulating proteins observed in this study are specific to Dox or whether they are also present in other types of heart failure, representing an important area of future investigation. In addition, given that our patient cohorts consisted exclusively of female patients, future studies will focus on characterizing sex-specific differences in Dox-associated Hpx signaling in both the clinical and preclinical setting.

Given the increasing burden of both heart failure and cancer in the aging population, the identification of new mechanisms of cardiac toxicity that can be interrogated directly in patients has the potential to improve risk stratification and cardioprotection in the growing population of cancer survivors. These findings motivate additional studies to assess whether the Hpx pathway could be leveraged for therapeutic benefit in patients at risk of anthracycline cardiomyopathy.

MATERIALS AND METHODS

Patient studies

Patients >18 years of age diagnosed with HER2-positive breast cancer and scheduled to receive adjuvant therapy (anthracyclines, taxanes, and trastuzumab) were recruited prospectively and consecutively from the Massachusetts General Hospital, MD Anderson Cancer Center, and McGill University, as previously reported (discovery cohort) (*50*, *51*). The study was approved by the institutional review board of the participating institutions, and all participants gave informed consent. The typical cancer treatment regimen consisted of Dox (60 mg/m^2) and cyclophosphamide (600 mg/m^2) every 3 weeks for 4 cycles [dose-dense doxorubicin and cyclophosphamide (ddAC)]. At 3 months, all patients received paclitaxel (80 mg/m^2) and trastuzumab (2 mg/kg) weekly for 12 weeks, followed by trastuzumab (6 mg/kg) every 3 weeks for 1 year. Questionnaires were administered, fasting blood samples were collected, and transthoracic echocardiograms were obtained every 3 months during the study period. Patients with LVEF of <50% before chemotherapy or those who were unwilling or unable to provide informed consent were excluded at the time of enrollment.

LVEF and GLS were measured as previously described (*50*). The same ultrasound machine was used to acquire all echocardiograms for each patient. All echocardiograms were assessed for LVEF and GLS by the same two readers, who were blinded to each other's measurements and to the patient visit number. The LVEF was calculated from the apical four- and two-chamber views using a modified Simpson's biplane method, which was the accepted method for LVEF measurement at the time of patient enrollment (2005–2010). GLS was measured using speckle tracking (EchoPAC; GE Medical, Milwaukee, WI), at a frame rate of 80 to 100 frames/s, and was calculated by averaging the values of peak systolic strain in the basal and midventricular segments of the four- and two-chamber views. The intraobserver variability for GLS measurement in the laboratory, reported as the mean error ± SD of 10 measurements, was previously measured as −0.58 ± 6.5%, and the interobserver variability was 2.7 ± 7.9% (*52*).

Of the 81 original study participants, 30 patients were selected for the discovery cohort on the basis of the availability of GLS data and nonhemolyzed blood samples at baseline and at 3 months following initiation of chemotherapy (after completion of anthracyclines), enriching for study participants who developed clinical signs and symptoms of heart failure during the first year after anthracycline treatment. For 12 patients in the discovery cohort, plasma was also available 6 months following chemotherapy (after completion of combined taxane/trastuzumab therapy and during trastuzumab therapy alone).

Blood samples were obtained from a second cohort of patients treated with ddAC at Houston Methodist Hospital (validation cohort) through a material transfer agreement approved by Houston Methodist and Beth Israel Deaconess Medical Center (BIDMC). Thirty patients had breast cancer and one patient had endometrial cancer. The study was approved by the Houston Methodist institutional review board, and all participants gave informed consent. Blood was drawn at baseline (before chemotherapy) and 6 weeks following initiation of ddAC. Nonhemolyzed blood samples

from 31 patients were included. GLS was measured at baseline and at 3 months as part of routine clinical care.

Proteomics

A total of 1317 proteins were measured in plasma samples using an aptamer-based proteomic platform (SomaScan) according to the manufacturer's protocol, as previously described (*53*). Proteins were measured at baseline and at 3 months, following completion of anthracyclines. In a subset of patients ($n = 12$), proteins were also measured at 6 months, during treatment with trastuzumab. Aptamers were assessed for specificity of binding to the protein of interest based on mass spectrometry, association with variants in the cognate gene in large population–based cohorts, correlation with an alternative proteomics platform (Olink), or ELISA.

Animal studies

Male and female C57BL/6 mice (strain code 027) aged 10 to 12 weeks were purchased from Charles River Laboratories. Hpx-deficient ($Hpx^{-/-}$) mating pairs were provided by B. Wegiel (BIDMC) and were originally generated by E. Tolosano (University of Torino, Italy) (*54*). All mice were housed in a specific pathogen–free barrier facility at BIDMC. Mice were maintained in a temperature- and humidity-controlled room on a 12-hour light/12-hour dark cycle with free access to food and water. Any animals that showed signs consistent with a moribund state were euthanized immediately. All animal procedures conformed to the Guide for the Care and Use of Laboratory Animals published by the U.S. National Institutes of Health and were approved by the BIDMC Animal Care and Use Committee.

In vivo drug administration and mouse treatment

Dox (3 mg/kg; Tocris Bioscience, 25316-40-9) or the corresponding vehicle (saline) was administered by intraperitoneal injection to 12-week-old male and female WT or $Hpx^{-/-}$ mice every 2 days for 2 weeks (total of eight injections) (*21*). Human Hpx (700 μg per mouse) was obtained from CSL Behring and was administered by intraperitoneal injection on the contralateral side to 12-week-old male WT mice every 2 days for 2 weeks, before each Dox injection. For the intravenous Dox model, Dox (5 mg/kg) or saline was administered once weekly for 4 weeks via tail vein. Echocardiography was performed 7 to 10 weeks after the initiation of Dox treatment, before harvest. For the intraperitoneal injection model, blood was collected through the submandibular vein 1 week before treatment (baseline), at day 14, and before harvest. For kinetic studies only, blood was collected from female mice through the submandibular vein on days 1, 3, 7, and 14 from the Dox initial dose (<100 μl per blood draw). For the intravenous injection model, blood was collected from female mice through the submandibular vein at baseline and at weeks 1, 2, 3, and 4. Body weight was measured at baseline and throughout the study. Heart weight and tibia length were measured after euthanasia. Heart and liver tissues were collected for Western blot, RT-qPCR, and immunostaining.

Echocardiography

A Vevo 2100 microultrasound imaging system (VisualSonics, Toronto, Canada) was used to perform conscious mouse echocardiography (*55*). Two-dimensional guided M-mode images were recorded in the short-axis view at the papillary muscle level to measure LV wall thickness and cavity dimensions. Percentage of fractional shortening (FS %) was calculated using the formula, FS (%) = (LVIDd − LVIDs/LVIDd) × 100. Conscious echocardiography was performed for all studies with the exception of treatment experiments with exogenous Hpx protein, where only sedated echocardiography was available.

Adult MHEC isolation

MHEC isolation was performed as described previously (*56*). Briefly, three to four mouse hearts were removed from adult mice aged 10 to 12 weeks; washed in 15 ml of cold isolation medium containing Dulbecco's modified Eagle's medium (DMEM), 20% fetal bovine serum (FBS), and 1% penicillin-streptomycin; minced finely with scissors; and digested in 25 ml of prewarmed collagenase B [50 mg into 25 ml of phosphate-buffered saline (PBS)] at 37°C for 45 to 60 min. During digestion, vortex was performed every 10 to 15 min, followed by the addition of 50 ml of isolation medium to stop the digestion. The digested tissue was filtered through a 70-μm cell strainer and centrifuged at 400*g* for 10 min at 4°C. The cell pellet was resuspended in 2 ml of cold PBS and incubated with platelet endothelial cell adhesion molecule–1 (PECAM-1/CD31; BD Biosciences, 553389)–coated Dynabeads (Thermo Fisher Scientific, 11035) at a concentration of 15 μl of beads per milliliter of cell suspension at room temperature for 10 min with end-over-end rotation. The tube containing cells was mounted on a magnetic separator and left for 1 to 2 min. The supernatant was then removed, and cells were resuspended in 10 ml of growth medium containing high-glucose DMEM with 20% FBS, 1% penicillin-streptomycin, heparin (100 μg/ml) (Sigma-Aldrich, H-3933), endothelial cell growth supplement (100 μg/ml) (BT-203, Sigma-Aldrich), 1× nonessential amino acids, 2 mM L-glutamine, 1× sodium pyruvate, and 25 mM Hepes. Cells with beads were plated in a gelatin-coated T75 flask. About 5 to 9 days later when cells approached confluence, the second sort with an identical protocol to the above was performed using intercellular adhesion molecule–2 (ICAM-2; BD Biosciences, 553325)–coated Dynabeads. MHECs from passages 2 to 5 were used for experiments.

Heart immune cell isolation

Heart immune cells were isolated as previously described (*56*). Briefly, the mouse heart was perfused with 20 ml of cold PBS before removal from the chest, minced into very small pieces, and digested in a 0.1% collagenase B solution (catalog no. LS004177, Worthington Biochemical Co.) for 30 min in a 37°C water bath with vortex every 10 min. After digestion, single cells were neutralized by RPMI 1640 supplemented with 10% FBS and were filtered through a 70-μm cell strainer. Heart immune cells were then separated using density gradient centrifugation in a 15-ml tube layered with 2 ml of 80% Percoll (17-0891-09, Thermo Fisher Scientific, Hampton, NH), 2 ml of 62% Percoll, 2 ml of 55% Percoll, and 3 ml of 45% Percoll that was premixed with the cell preparation. Cells were centrifuged at 800*g* for 30 min. Single cells between each layer were carefully obtained and washed with PBS twice.

Blood immune cell isolation

Blood was collected from the mouse heart, and 10 ml of 1× red blood cell lysis buffer (BioLegend, 20302) was applied followed by incubation in the dark for 10 min. After incubation, blood immune cells were then centrifuged at 600*g* for 6 min at room temperature and followed by washes with PBS twice.

Flow cytometry

Immune cells isolated from blood or heart were stained with CD45 (1:200; eBioscience, 45-0451-82), CD11b (1:200; eBioscience, 17-0112-82), CD64 (1:200; eBioscience, 12-0641-82), F4/80 (1:200; BioLegend, 123114), and Hpx (1:100; Invitrogen, PA5-13605) followed by incubation with goat anti-rabbit immunoglobulin G secondary antibody (1:500; Invitrogen, 31573). In each experiment, the appropriate isotype control monoclonal antibodies and single-conjugate controls were also included.

Enzyme-linked immunosorbent assay

Mouse plasma Hpx was measured using a commercially available ELISA kit (Abcam, ab157716) with a coefficient of variance (CV) of <10% for intra-assay precision. Human plasma Hpx was measured using a commercially available ELISA kit (Abcam, ab108859) with a CV of 5.8% for intra-assay precision. Mouse plasma IL-6 was measured using a commercially available ELISA kit (R&D Systems, M6000B) with a CV of <6.7% for intra-assay precision. All of these assays were performed as per manufacturer's instructions.

Immunostaining

Frozen sections of heart tissues (5-μm thickness) were fixed with cold acetone for 5 min followed by blocking of nonspecific binding of secondary antibody by incubation with PBS supplemented with 5% normal rabbit serum for 1 hour at room temperature. The heart section was then stained with LRP-1 antibody (1:200; Cell Signaling Technology, 26387S), CD31 (1:100; eBioscience, 11-0311-82), cardiac myosin heavy chain (1:200; Invitrogen, MA1-26180), or CD64 (1:100; Santa Cruz Biotechnology, sc-515431) at 4°C for overnight and followed by incubation of a secondary antibody (1:500; eBioscience, 4431S) at room temperature for 2 hours. Nuclei were stained with 4′,6-diamidino-2-phenylindole (DAPI). The sections were mounted and images were captured using an immunofluorescence microscope.

Table 3. Primer sequences used for RT-qPCR.

Gene (mouse)	Forward	Reverse
GAPDH	CATCACTGCCACCCAGAAG ACTG	ATGCCAGTGAGCTTCC CGTTCAG
Nppb	AAGCTGCTGGAGCTGATAA GA	GTTACAGCCCAAACGA CTGAC
Bax	TGAAGACAGGGGCCTTTTT G	AATTCGCCGGAGACAC TCG
Bcl2	GTCGCTACCGTCGT GACTTC	CAGACATGCACCTACC CAGC
Hpx	AGCAGTGGC GCTAAATATCCT	CCATTTTCAACTTC GGCAACTC
CXCR2	ATGCCCTCTATTCTGCCA GAT	GTGCTCCGGTTGTATA AGATGAC
CCL12	ATTTCCACACTTCTAT GCCTCCT	ATCCAGTATGGTCCTG AAGATCA
Irf5	GGTCAACGGGGAAAA GAAACT	CATCCACCCCTTCAGT GTACT
Nr4a1	GAGTTCGGCAA GCCTACCAT	GTGTACCCGTCCATGA AGGTG
Emr1	CCCCAGTGTCCTTACAGAG TG	GTGCCCAGAGTGGAT GTCT
Hbegf	CGGGGAGTGCAGATACCT G	TTCTCCACTGGTAGAG TCAGC
Pdgfc	GCCAAAGAACGGGGACTC G	AGTGACAACTCTCT CATGCCG
Ptgs2/ COX2	TTCAACACACTCTATCACT GGC	AGAAGCGTTTGC GGTACTCAT

Cardiomyocyte cross-sectional area staining and measurements

Heart sections were stained with WGA (5 μg/ml; RL-1022, Vectorlabs) for 10 min at 37°C, followed by fixation with 4% paraformaldehyde for 15 min at 37°C. After fixation, tissue sections were washed three times in PBS and followed by permeabilization of the cells with 0.2% Triton X-100 for subsequent counterstaining with DAPI. Images were acquired using an all-in-one fluorescence microscope (BZ-X710, Keyence). Cardiomyocyte cross-sectional area was measured by ImageJ. Measurements were performed in five to six regions of interest per section and 20 cells per region.

Western blot

Protein was extracted from heart and liver tissue using radioimmunoprecipitation assay lysis buffer (Thermo Fisher Scientific, 89900) and separated using 10% Criterion TGX Stain-Free Protein Gel (Bio-Rad, 5678034). The proteins were transferred to a nitrocellulose membrane (Bio-Rad, 1704159) using a Trans-Blot Turbo Transfer system (Bio-Rad, 1704150EDU). Membranes were incubated overnight at 4°C with primary antibodies Hpx (1:5000; R&D System, AF7007), HO-1 (1:1000; Abcam, ab13248), Nrf2 (1:1000; Abcam, ab137550), Ptgs2/COX2 (1:1000; R&D System, AF4198), GPX4 (1:2000; R&D System, MAB5457), cleaved caspase-3 (1:500; Cell Signaling Technology, 9654S), human Hpx (1:1000; R&D System, MAB4490), and rabbit anti-mouse glyceraldehyde-3-phosphate dehydrogenase (GAPDH) (1:1000; Cell Signaling Technology, 2118S) followed by incubation with their corresponding horseradish peroxidase (HRP)–conjugated secondary antibodies for 2 hours at room temperature. For cleaved caspase-3 detection in the heart, membranes were incubated with biotinylated rabbit cleaved caspase-3 monoclonal antibody for 36 hours at 4°C and followed by incubation with streptavidin-HRP for 2 hours at room temperature. Antibodies used in heart cleaved caspase-3 detection were diluted using a SignalBoost immunoreaction enhancer kit (Millipore, 407207). The resulting signals were detected using the Western ECL Substrate (Bio-Rad, 1705061). GAPDH was used to ensure equal protein loading.

Reverse transcription quantitative polymerase chain reaction

Total RNA was extracted from cardiac LV tissue or liver using TRIzol reagent (Thermo Fisher Scientific, 15596018), and complementary DNA (cDNA) was synthesized using the high-capacity cDNA reverse transcription kit (Bio-Rad, 1725038). The relative mRNA levels of target genes were quantified using the Applied Biosystems PowerUp SYBR Green Master Mix (Thermo Fisher Scientific, A25742). Each reaction was performed in duplicate, and changes in relative gene expression levels were normalized to

GAPDH levels using the $2^{-\Delta\Delta CT}$ method. Primer sequences are listed in Table 3.

Heme measurement

Blood collected from the submandibular vein after 2-week Dox treatment was centrifuged at 1000*g* for 30 min to obtain plasma. Blood and plasma heme levels were measured using a commercially available kit (Abnova, KA1617) as per the manufacturer's instructions. Heme content in tissues was quantified by the method of Sassa described previously (*57*). Briefly, hearts were homogenized in PBS with 1% Triton X-100 solution (Sigma-Aldrich, 93443-100ML). Equal amounts of protein were incubated with 2 M oxalic acid for 30 min at 95°C and centrifuged to remove debris. Fluorescence of the supernatant was measured at excitation of 405 nm/emission of 600 nm.

NHI detection

Heart tissues were digested in 10-fold volume of acid solution containing 10% trichloroacetic acid and 3 M HCl at 65°C for 20 hours. NHI was quantified by a previously described colorimetric assay using bathophenanthroline disulfonate (*58*).

Lipid peroxidation and DCF detection

Heart lipid peroxidation and DCF were measured with a colorimetric assay kit (ab233471, Abcam) and fluorescence assay kit (STA-347, Cell Biolabs Inc.), respectively, according to the manufacturers' instructions.

Statistical analysis

For aptamer-based proteomics, protein levels were log-normalized, and the change in protein level at 3 and 6 months was compared to the change in GLS (absolute value) at 3 months for each patient using Pearson's correlation coefficient. The Benjamini-Hochberg method was used to correct for multiple comparisons. All mouse data were expressed as means ± SEM. Welch's *t* test was used to compare differences between two groups. Ordinary one-way analysis of variance (ANOVA) followed by the Tukey-Kramer test was used for multiple group comparisons. R and GraphPad Prism 8 were used for data analysis and figures, and $P < 0.05$ was considered significant.

Supplementary Materials

This PDF file includes:
Figs. S1 to S10

Other Supplementary Material for this manuscript includes the following:
Supplemental Data

REFERENCES AND NOTES

1. P. Vejpongsa, E. T. Yeh, Prevention of anthracycline-induced cardiotoxicity: Challenges and opportunities. *J. Am. Coll. Cardiol.* **64**, 938–945 (2014).
2. D. Cardinale, A. Colombo, G. Bacchiani, I. Tedeschi, C. A. Meroni, F. Veglia, M. Civelli, G. Lamantia, N. Colombo, G. Curigliano, C. Fiorentini, C. M. Cipolla, Early detection of anthracycline cardiotoxicity and improvement with heart failure therapy. *Circulation* **131**, 1981–1988 (2015).
3. G. H. Oliveira, M. Dupont, D. Naftel, S. L. Myers, Y. Yuan, W. H. Tang, G. Gonzalez-Stawinski, J. B. Young, D. O. Taylor, R. C. Starling, Increased need for right ventricular support in patients with chemotherapy-induced cardiomyopathy undergoing mechanical circulatory support: Outcomes from the INTERMACS Registry (Interagency Registry for Mechanically Assisted Circulatory Support). *J. Am. Coll. Cardiol.* **63**, 240–248 (2014).
4. D. Cardinale, M. T. Sandri, A. Colombo, N. Colombo, M. Boeri, G. Lamantia, M. Civelli, F. Peccatori, G. Martinelli, C. Fiorentini, C. M. Cipolla, Prognostic value of troponin I in cardiac risk stratification of cancer patients undergoing high-dose chemotherapy. *Circulation* **109**, 2749–2754 (2004).
5. B. G. Demissei, R. A. Hubbard, L. Zhang, A. M. Smith, K. Sheline, C. McDonald, V. Narayan, S. M. Domchek, A. DeMichele, P. Shah, A. S. Clark, K. Fox, J. Matro, A. R. Bradbury, H. Knollman, K. D. Getz, S. H. Armenian, J. L. Januzzi, W. H. W. Tang, P. Liu, B. Ky, Changes in cardiovascular biomarkers with breast cancer therapy and associations with cardiac dysfunction. *J. Am. Heart Assoc.* **9**, e014708 (2020).
6. E. Tolosano, F. Altruda, Hemopexin: Structure, function, and regulation. *DNA Cell Biol.* **21**, 297–306 (2002).
7. V. Hvidberg, M. B. Maniecki, C. Jacobsen, P. Højrup, H. J. Møller, S. K. Moestrup, Identification of the receptor scavenging hemopexin-heme complexes. *Blood* **106**, 2572–2579 (2005).
8. F. Vinchi, L. De Franceschi, A. Ghigo, T. Townes, J. Cimino, L. Silengo, E. Hirsch, F. Altruda, E. Tolosano, Hemopexin therapy improves cardiovascular function by preventing heme-induced endothelial toxicity in mouse models of hemolytic diseases. *Circulation* **127**, 1317–1329 (2013).
9. A. V. Menon, J. Liu, H. P. Tsai, L. Zeng, S. Yang, A. Asnani, J. Kim, Excess heme upregulates heme oxygenase 1 and promotes cardiac ferroptosis in mice with sickle cell disease. *Blood* **139**, 936–941 (2022).
10. Y. Ichikawa, M. Ghanefar, M. Bayeva, R. Wu, A. Khechaduri, S. V. Naga Prasad, R. K. Mutharasan, T. J. Naik, H. Ardehali, Cardiotoxicity of doxorubicin is mediated through mitochondrial iron accumulation. *J. Clin. Invest.* **124**, 617–630 (2014).
11. G. Curigliano, D. Lenihan, M. Fradley, S. Ganatra, A. Barac, A. Blaes, J. Herrmann, C. Porter, A. R. Lyon, P. Lancellotti, A. Patel, J. DeCara, J. Mitchell, E. Harrison, J. Moslehi, R. Witteles, M. G. Calabro, R. Orecchia, E. de Azambuja, J. L. Zamorano, R. Krone, Z. Iakobishvili, J. Carver, S. Armenian, B. Ky, D. Cardinale, C. M. Cipolla, S. Dent, K. Jordan; ESMO Guidelines Committee, Management of cardiac disease in cancer patients throughout oncological treatment: ESMO consensus recommendations. *Ann. Oncol.* **31**, 171–190 (2020).
12. J. D. Mosley, M. D. Benson, J. G. Smith, O. Melander, D. Ngo, C. M. Shaffer, J. F. Ferguson, M. S. Herzig, C. A. McCarty, C. G. Chute, G. P. Jarvik, A. S. Gordon, M. R. Palmer, D. R. Crosslin, E. B. Larson, D. S. Carrell, I. J. Kullo, J. A. Pacheco, P. L. Peissig, M. H. Brilliant, T. E. Kitchner, J. G. Linneman, B. Namjou, M. S. Williams, M. D. Ritchie, K. M. Borthwick, K. Kiryluk, F. D. Mentch, P. M. Sleiman, E. W. Karlson, S. S. Verma, Y. Zhu, R. S. Vasan, Q. Yang, J. C. Denny, D. M. Roden, R. E. Gerszten, T. J. Wang, Probing the virtual proteome to identify novel disease biomarkers. *Circulation* **138**, 2469–2481 (2018).
13. V. Emilsson, M. Ilkov, J. R. Lamb, N. Finkel, E. F. Gudmundsson, R. Pitts, H. Hoover, V. Gudmundsdottir, S. R. Horman, T. Aspelund, L. Shu, V. Trifonov, S. Sigurdsson, A. Manolescu, J. Zhu, Ö. Olafsson, J. Jakobsdottir, S. A. Lesley, J. To, J. Zhang, T. B. Harris, L. J. Launer, B. Zhang, G. Eiriksdottir, X. Yang, A. P. Orth, L. L. Jennings, V. Gudnason, Co-regulatory networks of human serum proteins link genetics to disease. *Science* **361**, 769–773 (2018).
14. K. Suhre, M. Arnold, A. M. Bhagwat, R. J. Cotton, R. Engelke, J. Raffler, H. Sarwath, G. Thareja, A. Wahl, R. K. DeLisle, L. Gold, M. Pezer, G. Lauc, M. A. El-Din Selim, D. O. Mook-Kanamori, E. K. Al-Dous, Y. A. Mohamoud, J. Malek, K. Strauch, H. Grallert, A. Peters, G. Kastenmüller, C. Gieger, J. Graumann, Connecting genetic risk to disease end points through the human blood plasma proteome. *Nat. Commun.* **8**, 14357 (2017).
15. B. B. Sun, J. C. Maranville, J. E. Peters, D. Stacey, J. R. Staley, J. Blackshaw, S. Burgess, T. Jiang, E. Paige, P. Surendran, C. Oliver-Williams, M. A. Kamat, B. P. Prins, S. K. Wilcox, E. S. Zimmerman, A. Chi, N. Bansal, S. L. Spain, A. M. Wood, N. W. Morrell, J. R. Bradley, N. Janjic, D. J. Roberts, W. H. Ouwehand, J. A. Todd, N. Soranzo, K. Suhre, D. S. Paul, C. S. Fox, R. M. Plenge, J. Danesh, H. Runz, A. S. Butterworth, Genomic atlas of the human plasma proteome. *Nature* **558**, 73–79 (2018).
16. M. D. Benson, Q. Yang, D. Ngo, Y. Zhu, D. Shen, L. A. Farrell, S. Sinha, M. J. Keyes, R. S. Vasan, M. G. Larson, J. G. Smith, T. J. Wang, R. E. Gerszten, Genetic architecture of the cardiovascular risk proteome. *Circulation* **137**, 1158–1172 (2018).
17. C. A. Geisberg, W. M. Abdallah, M. da Silva, C. Silverstein, H. M. Smith, V. Abramson, I. Mayer, J. Means-Powell, D. Freehardt, B. White, D. Lenihan, D. B. Sawyer, Circulating neuregulin during the transition from stage A to stage B/C heart failure in a breast cancer cohort. *J. Card. Fail.* **19**, 10–15 (2013).
18. A. Asnani, B. Zheng, Y. Liu, Y. Wang, H. H. Chen, A. Vohra, A. Chi, I. Cornella-Taracido, H. Wang, D. G. Johns, D. E. Sosnovik, R. T. Peterson, Highly potent visnagin derivatives inhibit Cyp1 and prevent doxorubicin cardiotoxicity. *JCI Insight.* **3**, (2018).
19. J. Zhu, J. Zhang, L. Zhang, R. Du, D. Xiang, M. Wu, R. Zhang, W. Han, Interleukin-1 signaling mediates acute doxorubicin-induced cardiotoxicity. *Biomed. Pharmacother.* **65**, 481–485 (2011).

20. A. Asnani, X. Shi, L. Farrell, R. Lall, I. A. Sebag, J. C. Plana, R. E. Gerszten, M. Scherrer-Crosbie, Changes in citric acid cycle and nucleoside metabolism are associated with anthracycline cardiotoxicity in patients with breast cancer. *J. Cardiovasc. Transl. Res.* **13**, 349–356 (2020).
21. D. Amgalan, T. P. Garner, R. Pekson, X. F. Jia, M. Yanamandala, V. Paulino, F. G. Liang, J. J. Corbalan, J. Lee, Y. Chen, G. S. Karagiannis, L. R. Sanchez, H. Liang, S. R. Narayanagari, K. Mitchell, A. Lopez, V. Margulets, M. Scarlata, G. Santulli, A. Asnani, R. T. Peterson, R. B. Hazan, J. S. Condeelis, M. H. Oktay, U. Steidl, L. A. Kirshenbaum, E. Gavathiotis, R. N. Kitsis, A small-molecule allosteric inhibitor of BAX protects against doxorubicin-induced cardiomyopathy. *Nat. Cancer.* **1**, 315–328 (2020).
22. S. Immenschuh, D. X. Song, H. Satoh, U. Muller-Eberhard, The type II hemopexin interleukin-6 response element predominates the transcriptional regulation of the hemopexin acute phase responsiveness. *Biochem. Biophys. Res. Commun.* **207**, 202–208 (1995).
23. D. L. Li, Z. V. Wang, G. Ding, W. Tan, X. Luo, A. Criollo, M. Xie, N. Jiang, H. May, V. Kyrychenko, J. W. Schneider, T. G. Gillette, J. A. Hill, Doxorubicin blocks cardiomyocyte autophagic flux by inhibiting lysosome acidification. *Circulation* **133**, 1668–1687 (2016).
24. H. Mao, P. Lockyer, L. Li, C. M. Ballantyne, C. Patterson, L. Xie, X. Pi, Endothelial LRP1 regulates metabolic responses by acting as a co-activator of PPARγ. *Nat. Commun.* **8**, 14960 (2017).
25. W. P. Lafuse, D. J. Wozniak, M. V. S. Rajaram, Role of cardiac macrophages on cardiac inflammation, fibrosis and tissue repair. *Cell* **10**, 51 (2020).
26. X. Fang, H. Wang, D. Han, E. Xie, X. Yang, J. Wei, S. Gu, F. Gao, N. Zhu, X. Yin, Q. Cheng, P. Zhang, W. Dai, J. Chen, F. Yang, H. T. Yang, A. Linkermann, W. Gu, J. Min, F. Wang, Ferroptosis as a target for protection against cardiomyopathy. *Proc. Natl. Acad. Sci. U.S.A.* **116**, 2672–2680 (2019).
27. G. Ingoglia, C. M. Sag, N. Rex, L. De Franceschi, F. Vinchi, J. Cimino, S. Petrillo, S. Wagner, K. Kreitmeier, L. Silengo, F. Altruda, L. S. Maier, E. Hirsch, A. Ghigo, E. Tolosano, Hemopexin counteracts systolic dysfunction induced by heme-driven oxidative stress. *Free Radic. Biol. Med.* **108**, 452–464 (2017).
28. D. Tang, X. Chen, R. Kang, G. Kroemer, Ferroptosis: Molecular mechanisms and health implications. *Cell Res.* **31**, 107–125 (2021).
29. H. Ouled-Haddou, K. Messaoudi, Y. Demont, R. Lopes Dos Santos, C. Carola, A. Caulier, P. Vong, N. Jankovsky, D. Lebon, A. Willaume, J. Demagny, T. Boyer, J. P. Marolleau, J. Rochette, L. Garcon, A new role of glutathione peroxidase 4 during human erythroblast enucleation. *Blood Adv.* **4**, 5666–5680 (2020).
30. S. Kumar, U. Bandyopadhyay, Free heme toxicity and its detoxification systems in human. *Toxicol. Lett.* **157**, 175–188 (2005).
31. F. Vinchi, M. Costa da Silva, G. Ingoglia, S. Petrillo, N. Brinkman, A. Zuercher, A. Cerwenka, E. Tolosano, M. U. Muckenthaler, Hemopexin therapy reverts heme-induced proinflammatory phenotypic switching of macrophages in a mouse model of sickle cell disease. *Blood* **127**, 473–486 (2016).
32. G. M. Vercellotti, P. Zhang, J. Nguyen, F. Abdulla, C. Chen, P. Nguyen, C. Nowotny, C. J. Steer, A. Smith, J. D. Belcher, Hepatic overexpression of hemopexin inhibits inflammation and vascular stasis in murine models of sickle cell disease. *Mol. Med.* **22**, 437–451 (2016).
33. J. D. Belcher, C. Chen, J. Nguyen, F. Abdulla, P. Zhang, H. Nguyen, P. Nguyen, T. Killeen, S. M. Miescher, N. Brinkman, K. A. Nath, C. J. Steer, G. M. Vercellotti, Haptoglobin and hemopexin inhibit vaso-occlusion and inflammation in murine sickle cell disease: Role of heme oxygenase-1 induction. *PLOS ONE* **13**, e0196455 (2018).
34. Y. I. Miller, A. Smith, W. T. Morgan, N. Shaklai, Role of hemopexin in protection of low-density lipoprotein against hemoglobin-induced oxidation. *Biochemistry* **35**, 13112–13117 (1996).
35. V. Poillerat, T. Gentinetta, J. Leon, A. Wassmer, M. Edler, C. Torset, D. Luo, G. Tuffin, L. T. Roumenina, Hemopexin as an inhibitor of hemolysis-induced complement activation. *Front. Immunol.* **11**, 1684 (2020).
36. H. Zhang, A. Xu, X. Sun, Y. Yang, L. Zhang, H. Bai, J. Ben, X. Zhu, X. Li, Q. Yang, Z. Wang, W. Wu, D. Yang, Y. Zhang, Y. Xu, Q. Chen, Self-maintenance of cardiac resident reparative macrophages attenuates doxorubicin-induced cardiomyopathy through the SR-A1-c-Myc axis. *Circ. Res.* **127**, 610–627 (2020).
37. E. Mantuano, C. Brifault, M. S. Lam, P. Azmoon, A. S. Gilder, S. L. Gonias, LDL receptor-related protein-1 regulates NFκB and microRNA-155 in macrophages to control the inflammatory response. *Proc. Natl. Acad. Sci. U.S.A.* **113**, 1369–1374 (2016).
38. L. Vi, G. S. Baht, E. J. Soderblom, H. Whetstone, Q. Wei, B. Furman, V. Puviindran, P. Nadesan, M. Foster, R. Poon, J. P. White, Y. Yahara, A. Ng, T. Barrientos, M. Grynpas, M. A. Mosely, B. A. Alman, Macrophage cells secrete factors including LRP1 that orchestrate the rejuvenation of bone repair in mice. *Nat. Commun.* **9**, 5191 (2018).
39. S. E. Lipshultz, S. R. Lipsitz, J. L. Kutok, T. L. Miller, S. D. Colan, D. S. Neuberg, K. E. Stevenson, M. D. Fleming, S. E. Sallan, V. I. Franco, J. M. Henkel, B. L. Asselin, U. H. Athale, L. A. Clavell, B. Michon, C. Laverdiere, E. Larsen, K. M. Kelly, L. B. Silverman, Impact of hemochromatosis gene mutations on cardiac status in doxorubicin-treated survivors of childhood high-risk leukemia. *Cancer* **119**, 3555–3562 (2013).
40. C. J. Miranda, H. Makui, R. J. Soares, M. Bilodeau, J. Mui, H. Vali, R. Bertrand, N. C. Andrews, M. M. Santos, Hfe deficiency increases susceptibility to cardiotoxicity and exacerbates changes in iron metabolism induced by doxorubicin. *Blood* **102**, 2574–2580 (2003).
41. X. Fang, H. Ardehali, J. Min, F. Wang, The molecular and metabolic landscape of iron and ferroptosis in cardiovascular disease. *Nat. Rev. Cardiol.* , (2022).
42. M. Maiorino, M. Conrad, F. Ursini, GPx4, lipid peroxidation, and cell death: Discoveries, rediscoveries, and open issues. *Antioxid. Redox Signal.* **29**, 61–74 (2018).
43. W. S. Yang, R. SriRamaratnam, M. E. Welsch, K. Shimada, R. Skouta, V. S. Viswanathan, J. H. Cheah, P. A. Clemons, A. F. Shamji, C. B. Clish, L. M. Brown, A. W. Girotti, V. W. Cornish, S. L. Schreiber, B. R. Stockwell, Regulation of ferroptotic cancer cell death by GPX4. *Cell* **156**, 317–331 (2014).
44. X. Xiao, Y. Jiang, W. Liang, Y. Wang, S. Cao, H. Yan, L. Gao, L. Zhang, miR-212-5p attenuates ferroptotic neuronal death after traumatic brain injury by targeting Ptgs2. *Mol. Brain* **12**, 78 (2019).
45. M. Li, V. Sala, M. C. De Santis, J. Cimino, P. Cappello, N. Pianca, A. Di Bona, J. P. Margaria, M. Martini, E. Lazzarini, F. Pirozzi, L. Rossi, I. Franco, J. Bornbaum, J. Heger, S. Rohrbach, A. Perino, C. G. Tocchetti, B. H. F. Lima, M. M. Teixeira, P. E. Porporato, R. Schulz, A. Angelini, M. Sandri, P. Ameri, S. Sciarretta, R. C. P. Lima-Júnior, M. Mongillo, T. Zaglia, F. Morello, F. Novelli, E. Hirsch, A. Ghigo, Phosphoinositide 3-kinase gamma inhibition protects from anthracycline cardiotoxicity and reduces tumor growth. *Circulation* **138**, 696–711 (2018).
46. B. N. Zordoky, A. Anwar-Mohamed, M. E. Aboutabl, A. O. El-Kadi, Acute doxorubicin toxicity differentially alters cytochrome P450 expression and arachidonic acid metabolism in rat kidney and liver. *Drug Metab. Dispos.* **39**, 1440–1450 (2011).
47. S. Zhang, X. Liu, T. Bawa-Khalfe, L. S. Lu, Y. L. Lyu, L. F. Liu, E. T. Yeh, Identification of the molecular basis of doxorubicin-induced cardiotoxicity. *Nat. Med.* **18**, 1639–1642 (2012).
48. G. Canesin, A. Di Ruscio, M. Li, S. Ummarino, A. Hedblom, R. Choudhury, A. Krzyzanowska, E. Csizmadia, M. Palominos, A. Stiehm, A. Ebralidze, S. Y. Chen, M. A. Bassal, P. Zhao, E. Tolosano, L. Hurley, A. Bjartell, D. G. Tenen, B. Wegiel, Scavenging of labile heme by hemopexin is a key checkpoint in cancer growth and metastases. *Cell Rep.* **32**, 108181 (2020).
49. S. M. Swain, F. S. Whaley, M. S. Ewer, Congestive heart failure in patients treated with doxorubicin. *Cancer* **97**, 2869–2879 (2003).
50. H. Sawaya, I. A. Sebag, J. C. Plana, J. L. Januzzi, B. Ky, T. C. Tan, V. Cohen, J. Banchs, J. R. Carver, S. E. Wiegers, R. P. Martin, M. H. Picard, R. E. Gerszten, E. F. Halpern, J. Passeri, I. Kuter, M. Scherrer-Crosbie, Assessment of echocardiography and biomarkers for the extended prediction of cardiotoxicity in patients treated with anthracyclines, taxanes, and trastuzumab. *Circ. Cardiovasc. Imaging* **5**, 596–603 (2012).
51. B. Ky, M. Putt, H. Sawaya, B. French, J. L. Januzzi, I. A. Sebag, J. C. Plana, V. Cohen, J. Banchs, J. R. Carver, S. E. Wiegers, R. P. Martin, M. H. Picard, R. E. Gerszten, E. F. Halpern, J. Passeri, I. Kuter, M. Scherrer-Crosbie, Early increases in multiple biomarkers predict subsequent cardiotoxicity in patients with breast cancer treated with doxorubicin, taxanes, and trastuzumab. *J. Am. Coll. Cardiol.* **63**, 809–816 (2014).
52. H. Sawaya, I. A. Sebag, J. C. Plana, J. L. Januzzi, B. Ky, V. Cohen, S. Gosavi, J. R. Carver, S. E. Wiegers, R. P. Martin, M. H. Picard, R. E. Gerszten, E. F. Halpern, J. Passeri, I. Kuter, M. Scherrer-Crosbie, Early detection and prediction of cardiotoxicity in chemotherapy-treated patients. *Am. J. Cardiol.* **107**, 1375–1380 (2011).
53. D. Ngo, S. Sinha, D. Shen, E. W. Kuhn, M. J. Keyes, X. Shi, M. D. Benson, J. F. O'Sullivan, H. Keshishian, L. A. Farrell, M. A. Fifer, R. S. Vasan, M. S. Sabatine, M. G. Larson, S. A. Carr, T. J. Wang, R. E. Gerszten, Aptamer-based proteomic profiling reveals novel candidate biomarkers and pathways in cardiovascular disease. *Circulation* **134**, 270–285 (2016).
54. E. Tolosano, E. Hirsch, E. Patrucco, C. Camaschella, R. Navone, L. Silengo, F. Altruda, Defective recovery and severe renal damage after acute hemolysis in hemopexin-deficient mice. *Blood* **94**, 3906–3914 (1999).
55. J. N. Rottman, G. Ni, M. Brown, Echocardiographic evaluation of ventricular function in mice. *Echocardiography* **24**, 83–89 (2007).
56. J. Liu, C. Yang, T. Liu, Z. Deng, W. Fang, X. Zhang, J. Li, Q. Huang, C. Liu, Y. Wang, D. Yang, G. K. Sukhova, J. S. Lindholt, A. Diederichsen, L. M. Rasmussen, D. Li, G. Newton, F. W. Luscinskas, L. Liu, P. Libby, J. Wang, J. Guo, G. P. Shi, Eosinophils improve cardiac function after myocardial infarction. *Nat. Commun.* **11**, 6396 (2020).
57. P. R. Sinclair, N. Gorman, J. M. Jacobs, Measurement of heme concentration. *Curr. Protoc. Toxicol.* **Chapter 8**, Unit 8.3 (2001).
58. J. D. Torrance, T. H. Bothwell, A simple technique for measuring storage iron concentrations in formalinised liver samples. *S. Afr. J. Med. Sci.* **33**, 9–11 (1968).

Acknowledgments: We thank S. Fisch from the Cardiovascular Physiology Core at the Brigham and Women's Hospital (Boston) for mouse echocardiography training; D. Amgalan and R. Kitsis from the Departments of Medicine/Cardiology and Cell Biology, Albert Einstein College of Medicine (New York) for technical expertise in *Bax*/*Bcl2* measurement; B. Wegiel from the Department of Surgery, BIDMC (Boston) for providing founder *Hpx*$^{-/-}$ mice; and A. N. R. Diaz, BIDMC for assisting with the analysis of patient data. **Funding:** This work was supported by

National Institutes of Health grants K08HL145019 and R01HL163172 (both to A.A.) and American Heart Association Postdoctoral Fellowship #20POST35210968 (to J.L.). **Author contributions:** J.L., R.L., and A.A. designed the study and interpreted the primary data. A.A., L.F., R.A.-G., M.S.-C., B.H.T., and R.E.G. enrolled patients and performed experiments to measure circulating proteins in patients. J.L., S.L., and R.L. performed most of the mouse experiments and data analysis. M.R., E.T., and A.G. performed exogenous Hpx treatment experiments in mice and analyzed the echo data. M.D.C. and J.K. measured NHI and assisted with interpretation of NHI and heme results. C.C. assisted with leukocyte sorting and profiling. All authors provided critical input into the drafting of the manuscript. **Competing interests:** A.A. has consulted or served on an advisory board for Sanofi, AstraZeneca, and Cytokinetics and serves as the principal investigator on a sponsored research agreement with Genentech, all unrelated to the current work. A.G. is a cofounder and board member of Kither Biotech, a pharmaceutical product company developing PI3K inhibitors for the treatment of respiratory diseases not in conflict with statements present in this article. The other authors declare that they have no competing interests. **Data and materials availability:** All data needed to evaluate the conclusions in the paper are present in the paper and/or the Supplementary Materials. Purified Hpx protein can be provided by CSL Behring pending scientific review and a completed material transfer agreement. Requests for Hpx protein should be submitted directly to CSL Behring.

Submitted 9 May 2022
Accepted 29 November 2022
Published 23 December 2022
10.1126/sciadv.adc9245